beverages

MDPI

Article

Batch-Scale Simulation of Heat and Mass Transfer of Coffee Roasting in Spouted Bed Roasters

Mark Al-Shemmeri [1,2], Peter J. Fryer [2,*], Robert Farr [3] and Estefania Lopez-Quiroga [2]

[1] JDE Peet's, R&D, 3571 NA Utrecht, The Netherlands
[2] School of Chemical Engineering, University of Birmingham, Birmingham B15 2TT, UK; e.lopez-quiroga@bham.ac.uk
[3] JDE Peet's, R&D, Banbury OX16 2QU, UK
* Correspondence: p.j.fryer@bham.ac.uk

Abstract

Understanding heat and mass transfer phenomena is fundamental to successful roasting practices. These phenomena can be quantified via an energy balance over the roaster, whereby heat and mass transfer equations can be formulated. Through rigorous calibration of the simulation with experimentally derived data obtained using a spouted bed roaster, a zero-dimensional, batch-scale model of coffee roasting was developed to predict time–temperature roasting profiles. Calibration involved implementation of (i) an airflow calibration to determine the air mass flow rate and velocity of air input to the roaster, (ii) kinetic models and empirical correlations to describe coffee's physicochemical development during roasting and (iii) a non-linear least squares fitting procedure to estimate system-dependent parameters—such as the thermal response coefficient and heat transfer effectiveness—that are otherwise difficult to determine. In this way, user inputs of roasting parameters relevant for spouted bed roasters—batch size, airflow and inlet air temperature—were probed to capture the full kinetics of coffee roasting under various process conditions, from which rate constants for mass loss kinetics were determined. In this study, development of the zero-dimensional, batch-scale simulation is described, alongside rigorous calibration with pilot-scale roasting trials. These simulations are application-ready and can be used by product and process developers to roast coffee in silico, providing not just an informative tool, but one that can be instructive and predict requirements for raw material (green coffee) properties, roasting process conditions, or roasted coffee properties.

Keywords: coffee; roasting; temperature prediction; simulation; spouted bed roaster

check for updates

Received: 10 September 2025
Revised: 22 October 2025
Accepted: 3 November 2025
Published: 17 November 2025

Citation: Al-Shemmeri, M.; Fryer, P.J.; Farr, R.; Lopez-Quiroga, E. Batch-Scale Simulation of Heat and Mass Transfer of Coffee Roasting in Spouted Bed Roasters. *Beverages* **2025**, *11*, 162. https://doi.org/10.3390/beverages11060162

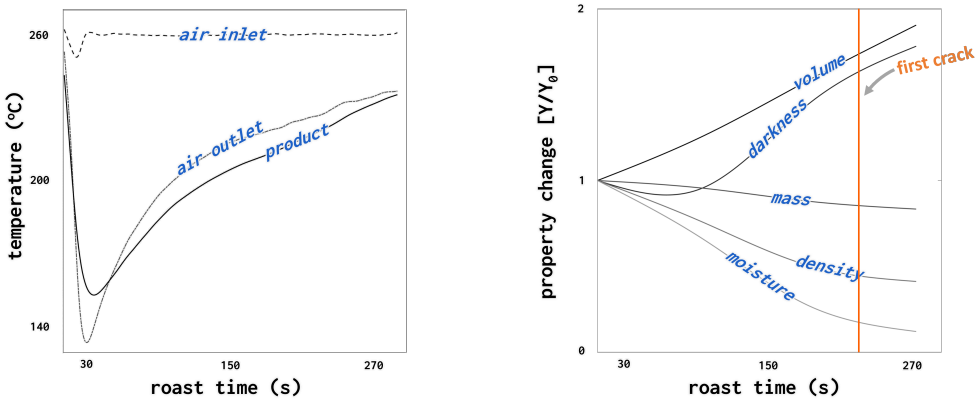
Copyright: © 2025 by the authors. Licensee MDPI, Basel, Switzerland. This article is an open access article distributed under the terms and conditions of the Creative Commons Attribution (CC BY) license (https://creativecommons.org/licenses/by/4.0/).

1. Introduction

1.1. Coffee's Physicochemical Transformation

Coffee roasting is a thermally driven process in which batches of green beans receive controlled time–temperature treatment, initiating a series of complex physicochemical transformations. These changes affect moisture content, porosity, density, colour, flavour and aroma [1,2]. As temperature surpasses 170–190 °C, Maillard and caramelisation reactions dominate, producing browning and aroma precursors while water vapour and CO_2 generation drive bean expansion and structural fracturing—otherwise known as 'first crack' [3,4]. Continued heating accelerates thermal decomposition, influencing acidity, volatile aromas and flavour balance [5–8]. Controlled heat input and timely cooling are, therefore, essential to achieve target sensory profiles and prevent post-roast reactions [9,10].

A representative roasting profile is illustrated in Figure 1a, with the relevant physical and chemical changes shown in Figure 1b.



(**a**) Time–Temp. Profile (**b**) Coffee Transformation

Figure 1. Example of (**a**) a time–temperature profile obtained by roasting under constant thermal load in a spouted bed roaster and (**b**) coffee's subsequent physicochemical transformation during roasting.

Regarding the effects roasting has on the chemistry of the bean and the resulting flavour profile of the coffee produced, Obando and Figueroa [6], Marek et al. [11], Gancarz et al. [12], Várady et al. [13], Febrianto and Zhu [14], Santanatoglia et al. [15] demonstrate these complexities—readers are particularly referred to a review of quality determinants in coffee production [16] and a recent review of coffee flavour [17].

Numerous empirical studies have quantified the kinetics of mass and moisture loss during roasting, highlighting the strong dependence of transformation rates on the applied time–temperature profile [2,3,10,18–29]. Recent work has also demonstrated links between porosity development and thermal properties [30]. These datasets form the foundation for empirical and semi-empirical models that describe roasting dynamics and offer calibration data for simulation frameworks [10,28].

1.2. Modelling and Simulation of Coffee Roasting

Mathematical models of roasting vary in complexity depending on their application. Batch-scale, zero-dimensional models predict bed-mean particle temperatures, yet cannot resolve internal bean temperature gradients—they are computationally efficient and readily embedded within process control systems. Particle-scale, three-dimensional models capture detailed heat and mass transfer effects within the bean but are computationally demanding and difficult to validate experimentally [1,31,32].

Kinetic models using nth-order Arrhenius-type reaction rates are often used to predict the temperature-dependent physicochemical behaviour of many food systems [33,34] and have been used to characterise coffee's physicochemical development in different roasting systems, seen in Perrone et al. [7], Bustos-Vanegas et al. [10], Wang and Lim [20], Vargas-Elias et al. [23]. This modelling approach simplifies the complex reactions that take place during roasting by lumping the chemistry into an nth-order reaction rate [35]. Such formulations have been successfully applied to describe moisture and mass loss during roasting [23,36,37]. The ordinary differential equation for nth-order chemical reaction kinetics corresponding to the rate of change of a property Y (of arbitrary units), with respect to time, depends on the temperature-dependent rate constant:

$$\frac{dY(t)}{dt} = -k(T)Y(t)^n \quad (1)$$

Although different studies have reported varying reaction orders (n = 0–1), each yielded acceptable fits within experimental uncertainty [20,24,29].

The thermal evolution of batch roasters can be captured using energy balances that couple air and bean temperatures through effective heat transfer coefficients [38–40]. The legacy of Schwartzberg [36,38,39,41] provides the foundation for simulation of time–temperature roasting profiles. Energy balance over a metal-walled spouted bed roaster describes the coffee's temperature evolution during roasting:

$$\frac{dT_b}{dt} = \frac{G_a C_{p,a}(T_{a,i} - T_{a,o}) + m_{bs,db}(Q_r + \Delta H_v \frac{dX_b}{dt}) - Q_{am} + Q_{mb}}{m_{bs,db}(1 + X)C_{p,b}} \quad (2)$$

Figure 2 shows the expected difference between the thermocouple and bean temperature during roasting [36].

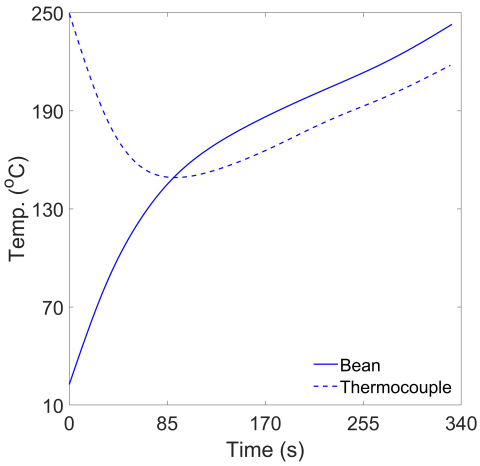


Figure 2. Simulated time–temperature profile corresponding to bean and thermocouple responses—resolved from a zero-dimensional heat and mass transfer model detailed in Section 2.2.5.

These models were further developed by [40,42–46] and further evolutions include CFD models [47] and porosity development [48]. Considering the effect of particle dynamics on heat transfer is a critical next step [49–52] that should also be considered during formulation of the thermal model.

Zero-dimensional, batch-scale simulations of heat and mass transfer are of most relevance to predictive process control systems due to their rapid solver times and ability to predict the effect of disturbances on the time–temperature profile in real-time—developers have a propensity for these models when developing digital shadows and twins.

2. Materials and Methods

The works of Schwartzberg [36,38,39,41] have been studied, adapted and developed by many to model and predict time–temperature profiles for several roasters of different scales and designs. This study used the described batch-scale energy balance (Equation (2)) to simulate time–temperature roasting profiles in a pilot-scale (0.5 kg) spouted bed roaster, making use of both kinetic models that describe coffee's mass and moisture loss and empirical correlations that enable prediction of thermophysical properties that are not easily measured. The simulation was calibrated with experimental data presented in Al-Shemmeri et al. [30] to increase its accuracy, robustness and applicability.

Therefore, to generate the tools useful for process and product development in a commercial setting, the workflow of the study is as follows:

- Data from our previous study [30] that detailed the physicochemical transformation of coffee during roasting are collated.

- Empirical data from roasting experiments are visualised to outline the evolution of temperature and physicochemical properties under different roasting conditions that establish the fundamental characteristics of the roaster.
- Physicochemical properties are correlated to generate equations that estimate more difficult-to-measure properties.
- Kinetic models of mass and moisture are developed using chemical reaction analogies with Arrhenius-type, temperature-dependent reaction rates and calibrated using the experimental data, with estimation of relevant rate coefficients that depend on process parameters.
- A zero-dimensional, batch-scale simulation of coffee's thermal evolution during roasting was formulated via energy balance.
- The sensitivity of the simulations to input factors (process parameters) and system-dependent parameters are assessed.
- The thermal model is then calibrated using empirical measurements of both the process and product as they evolve during roasting.
- After developing subroutines to correlate the estimated parameters with the input variables, predicted time–temperature profiles and corresponding physicochemical transformation rates are plotted for each of the case studies.

The present study does not intend to superimpose the chemistry onto the temperature profiles. The temperature regime needs to be known to be able to add the chemistry to the system. As the chemistry is complex and not likely robust to a lumped parameter approach—reducing the chemical transformation to a series of kinetic models—such complexity has not been attempted here.

2.1. Experimental Procedure

2.1.1. Green Coffee

A regional blend of Kenyan Arabica green coffee was selected and roasted by Al-Shemmeri et al. [30] to generate the experimental data used here for calibration of the simulations. The green coffee properties were not characterised according to the SCA green coffee classification or ICE/NYBOT Coffee "C" futures contract rules [53]; however, detailed characterisation of the coffee, including size, density, moisture and colour, are provided in Al-Shemmeri et al. [30].

2.1.2. Process Specification and Roasting Conditions

Pilot-scale roasting trials were performed using a spouted bed roaster (RFB-S, Neuhaus Neotec, Ganderkesee, Germany) in the R&D pilot plant of JDE Peet's (UK), as described in Al-Shemmeri et al. [30]. Two case studies relating to relevant process parameters were considered:

- (i) Case study I—Variation in constant inlet air temperature for a specified batch size and constant airflow.
- (ii) Case study II—Variation in batch size and airflow at a specified constant inlet air temperature.

In both studies, Kenyan Arabica coffee was roasted under constant (thermal load) process conditions to a surface (whole bean) colour of 70 ± 1 (ColorTrack arbitrary, native scale), confirmed in triplicate via colourimetry (ColorTrack Benchtop Device R-100B, FreshRoastSystems, Inc., Santa Clara, CA, USA). In case study I, batch sizes of 350.0 ± 0.1 g (Lunar, Acaia, Taipei, Taiwan) were roasted with a fan frequency of 48 Hz (corresponding to an airflow rate of 0.0228 kg s^{-1}—measured via anemometer as detailed in Appendix A) and constant inlet air temperatures of 220, 235, 250, 265 and 280 °C. In case study II, a constant inlet air temperature of 250 °C was used, with different batch size and airflow com-

binations such that the roaster's fan frequency ranged from 30 to 65 Hz (corresponding to airflow rates ranging 0.0141–0.0310 kg s^{-1}) for batch sizes between 200 and 500 g. To obtain time-series (i.e., kinetic) data, part-roasted coffees were obtained by varying roast time for each process condition, such that the coffee samples were obtained at equally distributed times between the start time, $t = 0$, and the final time, $t = t_{70}$ (rounded to the nearest integer). These roasting conditions are displayed in Table 1. In both case studies, once the specified roasting end-point was achieved, ambient air was used to cool the beans for 60 s. The roasted coffee was then packaged in valved, aluminium foil-laminated bags (Maxilla Packaging) and stored in a temperature controlled room (c. 20 °C) prior to characterisation.

Table 1. Process parameters corresponding to coffees roasted under different constant process conditions in a spouted bed roaster to a colour of 70 ± 1 at time, $t = t_{70}$.

Case Study	Batch Size (g)	Inlet Air Temp. (°C)	Fan Freq. (Hz)	Air Mass Flow Rate (kg s^{-1})	Roasting Times (s)
I	350	220	48	0.0228	0, 175, 350, 525, 700
I	350	235	48	0.0228	0, 104, 208, 312, 415
I	350	250	48	0.0228	0, 69, 138, 209, 278
I	350	265	48	0.0228	0, 54, 108, 164, 218
I	350	280	48	0.0228	0, 42, 84, 126, 168
II	200	250	30	0.0141	0, 75, 150, 225
II	200	250	48	0.0228	0, 52, 143, 215
II	200	250	65	0.0141	0, 58, 117, 175
II	350	250	39	0.0185	0, 109, 219, 328
II	350	250	48	0.0228	0, 93, 185, 278
II	350	250	65	0.0310	0, 85, 170, 255
II	500	250	48	0.0228	0, 115, 230, 345
II	500	250	65	0.0310	0, 107, 213, 320

2.1.3. Product Characterisation

For both case studies, the green and roasted coffee analyses included mass, intrinsic and packing density, moisture content, colour (whole bean), principal dimensions, volume and surface area. For roast and ground coffee analyses, coffees were ground using a flat burr grinder (EG1, Weber Workshops, Houston, TX, USA) and analyses included colour, thermal properties (thermal conductivity, specific heat capacity and thermal diffusivity) and median particle size (via laser diffraction). Grinding targeted a ground coffee median particle size, $x_{50} \approx 500$ µm, to reduce sample-to-sample variation.

The batch size of the green coffee was specified on a mass basis. The batch size of the roasted whole beans was determined after roasting, once cooled to ambient temperatures. Mass loss was the difference in the roasted batch's mass relative to the initial green bean batch size (i.e., $M_{loss} = 100\% \times \frac{(m_{b,s,0} - m_{b,s})}{m_{b,s,0}}$).

Coffee's moisture content was determined gravimetrically using a circulating oven (Model 100-800, Memmert, Schwabach, Germany) to dry the samples at 105 °C for 24 h. The samples were duplicated, with the measured values expressed in kg kg^{-1} (wet basis).

The principal dimensions (a (full-axis width), b (semi-axis depth) and c (full-axis length)) of whole bean coffees were measured using digital calipers (RS PRO, RS Components, Corby, UK). For each sample, 25 beans were measured. From principal dimensions, volume and surface area were calculated, assuming a hemi-ellipsoidal geometry:

$$V_b = \frac{4\pi(abc)^3}{6} \quad (3)$$

$$A_{s,b} \approx 2\pi\left(\frac{(0.5ab)^{1.6} + (0.25ac)^{1.6} + (0.5bc)^{1.6}}{3}\right)^{\frac{1}{1.6}} + \frac{\pi ac}{4} \quad (4)$$

For each of the 25 beans from the sample set, the individual bean mass was measured using a 0.1 mg precision balance (XSR204, Mettler-Toledo, Greifensee, Switzerland). In this way, the coffee bean's intrinsic density is as follows:

$$\rho_b = \frac{m_b}{V_b} \quad (5)$$

The green coffee's packing density (i.e., number of beans per unit mass), used later to estimate the total batch's surface area, was calculated from the cumulative measured mass of 50 coffee beans, performed in duplicate and expressed as number of beans per kg (kg^{-1}).

The whole bean and ground coffee colours were measured via reflectance (ColorTrack Benchtop Device R-100B, FreshRoastSystems, Inc., Santa Clara, CA, USA). A sample volume of 250 mL and sampling time of 60 s was used. Measurements were duplicated using aliquots of the sample, with the colour values expressed in arbitrary colour units.

The thermal properties (thermal conductivity, thermal diffusivity and volumetric heat capacity) of the ground (green, part-roasted and roasted) samples were determined using a thermal properties analyser (TEMPOS, METER Group, Pullman, DC, USA) using the SH-3 dual needle sensor. A total of 30 g of samples was poured freely into a 250 mL beaker. The SH-3 sensor was inserted into the sample through the beaker's wall (via pre-drilled holes) before the coffee bed was consolidated around the sensor using a 3D-printed tamper. Thermal properties were determined in duplicate over a 2 min sampling time.

Bean specific heat capacity was calculated from the measured thermal diffusivity, thermal conductivity and bulk density:

$$C_{p,b} = \frac{k_b}{\rho_{bulk} D_b} \quad (6)$$

2.2. Modelling

A zero-dimensional simulation was developed to predict the batch mean temperature and coffee's consequent physicochemical transformation during roasting. The approach is data-driven, such that measured process parameters and physical properties reduce the number of parameters that have to be estimated. Data from experimental case studies I and II were used for model calibration. In these experimental studies, the effect of batch size and airflow (case study II) on the time–temperature profiles (and subsequent physicochemical transformation) was greater than that of the inlet air temperature (case study I). Al-Shemmeri et al. [30] examined these data in detail. Case study II exhibited more diverse time–temperature profiles, especially at early times, compared to case study I. Consequently, for temperature-dependent kinetic models, training on the more diverse dataset proved more effective and robust for testing on a less diverse one. For calibration of models describing coffee's physiochemical transformation, data from case study II were first used to estimate model parameters, whilst data from case study I was later used to validate and assess the robustness of the generated models.

2.2.1. Coffee's Physicochemical Development

Using the chemical reaction analogy, whereby nth order reaction kinetics are combined with Arrhenius-type rate constants, coffee's physicochemical properties were likened to chemical concentrations and modelled using nth order reaction kinetics. For a given property with arbitrary units, Y, the rate of change (i.e., $\frac{dY}{dt}$) is a function of temperature,

reaction rate, activation energy, universal gas constant and reaction order index. The ordinary differential equation that governs the rate of change of Y is then [54]

$$\frac{dY}{dt} = -k_Y \exp\left(-\frac{E_a}{RT}\right) Y^n \tag{7}$$

For application to coffee's physicochemical transformation during roasting, two terms in Equation (7) were reconsidered. Firstly, temperature was assumed equal to the thermocouple temperature, which corresponds to the measurement of coffee beans and air in the roasting chamber. Whilst this will inherently reduce the accuracy and robustness of the estimated parameters, relative to the use of the actual bean temperature (which is more difficult to measure and validate in real roasting systems), this will enable developers to implement the generated models with no adaptation. Secondly, the units of the activation energy and universal gas constant can be confusing—how can the number of moles of coffee be quantified? To avoid this existential issue, the ratio of (E_a/R) is estimated [54,55].

In this way, Equation (7) applied here to the transformation of a coffee's intrinsic property (with arbitrary units in this example) during roasting becomes

$$\frac{dY}{dt} = -k_Y \exp\left(-\frac{E_a}{T_T}\right) Y^n \tag{8}$$

2.2.2. Thermal Balance at the Batch Scale

An energy balance over the roaster can be used to determine the batch mean (i.e., zero-dimensional) temperature evolution during roasting:

$$Q_b = (Q_{ab} + Q_{am}) - Q_{am} + Q_{mb} + Q_r + Q_e \tag{9}$$

where

$$\text{Bean temperature change:} \quad Q_b = m_{bs,db}(1 + X_b)C_{p,b}\frac{dT_b}{dt} \tag{10}$$

$$\text{Air temperature change:} \quad Q_{ab} + Q_{am} = G_a C_{p,a}(T_{a,i} - T_{a,o}) \tag{11}$$

$$\text{Heat loss from air to roaster:} \quad Q_{am} = h_{am}A_{am}(T_{a,i} - T_m) \tag{12}$$

$$\text{Heat loss from bean to roaster:} \quad Q_{mb} = h_{mb}A_{mb}(T_m - T_b) \tag{13}$$

$$\text{Heat generation:} \quad Q_r = \Delta H_r \frac{dm_{bs,db}}{dt} \tag{14}$$

$$\text{Evaporative cooling:} \quad Q_e = m_{bs,db}\Delta H_v \frac{dX_b}{dt} \tag{15}$$

To reduce the model complexity, the following assumptions were made:

- Heat transfer between the roaster's internal metal surfaces and the beans (i.e., conductive heat transfer) is negligible, as the metal–bean contact areas and times are low in spouted bed roasters—thus $Q_{mb} = 0$.
- Exothermic reactions are negligible prior to first crack (FC)—thus for $t \leq t_{FC}$, $Q_r = 0$.
- Roasting conditions induce particle dynamics that create a thermally homogenous bean bed, so bean-to-bean conductive and radiative heat transfer are negligible.
- The measured coffee bean moisture content, density, specific heat capacity and thermal conductivity correspond to the batch mean and they are representative of the total batch and are uniform within the bean.
- An equivalent coffee bean diameter represents the characteristic length for Nusselt number approximations, which were evaluated for spherical particles.

- Water enthalpy of vaporisation was assumed to occur at saturation pressure, dependent on water temperature; water temperature was assumed equal to that of the simulated bean (i.e., particle) temperature.

An adaptation of the energy balance proposed by Schwartzberg [36] based on the stated assumptions was used to predict the batch mean (i.e., zero-dimensional) temperature change during roasting:

$$\frac{dT_b}{dt} = \frac{G_a C_{p,a}(T_{a,i} - T_{a,o}) + m_{bs,db}(\Delta H_v \frac{dX_b}{dt}) - Q_{am}}{m_{bs,db}(1 + X_b)C_{p,b}} \tag{16}$$

The air temperature differential across the roaster is given by the following [36]:

$$(T_{a,i} - T_{a,o}) = (T_{a,i} - T_b)\left(1 - \exp\left(\frac{-\alpha_{ab} A_{ab}}{G_a C_{p,a}}\right)\right) \tag{17}$$

To account for the bean bed and the effects of particle dynamics on heat transfer, depicted in Figure 3, the overall heat transfer coefficient was modified as follows [36]:

$$\alpha_{ab} \approx \frac{h_{ab}}{1 + \eta_A Bi} \tag{18}$$

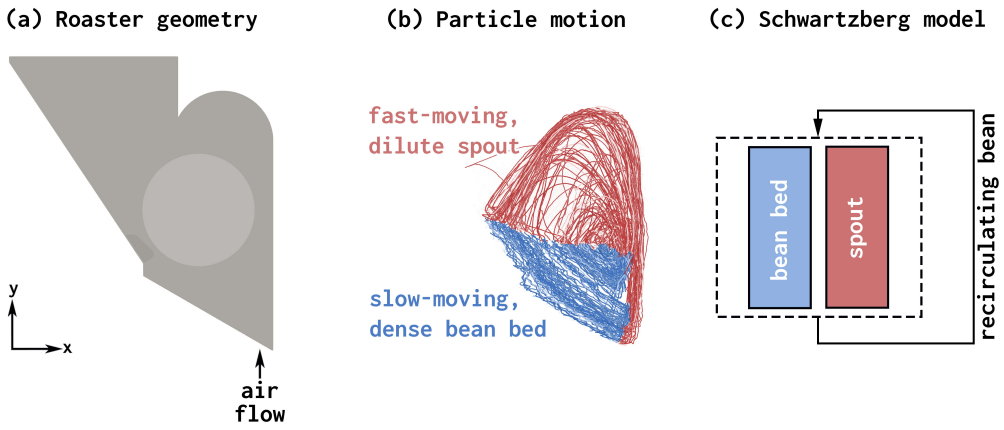


Figure 3. (**a**) Geometry of the spouted bed roaster, (**b**) coffee bean behaviour in the roaster [49], (**c**) heat transfer model using Schwartzberg approach.

The air-to-bean heat transfer coefficient can, therefore, be approximated via the Ranz-Marshall equation proposed by [56], which describes the flow of drying air around spherical particles:

$$Nu = \frac{h_{ab} d_b}{k_a} = 2 + 0.6 Re^{1/2} Pr^{1/3} \tag{19}$$

The thermal response coefficient was introduced to correct for the response time of the thermocouple in the roasting chamber. The thermocouple's temperature is thus

$$\frac{dT_T}{dt} = K(T_b - T_T) \tag{20}$$

2.2.3. Implementation of Physicochemical Transformation Models

For Equation (8), an initial value problem was implemented in MATLAB (2022a, Mathworks), with a non-linear least squares fitting procedure to estimate parameters (k_Y, E_a, n) using the Levenberg–Marquardt algorithm. The procedure (i) minimises the sum of squares according to the cost function, Δ_Y (i.e., the sum-of-squared differences between

experimental and simulated values), (ii) constrains parameters to specified bounds (as determined in Section 2.2.6 and (iii) was iterated three times to ensure a global minimum was located. The estimated parameters that yield the lowest relative error were used for validation and data visualisation.

Model coefficients for these equations were determined and incorporated explicitly in the heat transfer model.

2.2.4. Implementation of the Zero-Dimensional Heat Transfer Model

For the zero-dimensional heat transfer model, an initial value problem was implemented in MATLAB (2022a, Mathworks). According to the energy balance, there were three fittable parameters for the model: (i) the thermal response coefficient of the thermocouple, defined in Equation (20), (ii) the heat transfer effectiveness factor defined by [36] and defined in Equation (18), that accounts for the fact that some of the beans are not being heated, and (iii) the heat loss, noted in Equation (16).

The initial value problem (using the data values of Table 2) for four ordinary differential equations (ODEs), describing changes in the following:

- Mass (Equation (27)).
- Moisture (Equation (30)).
- Bean temperature (Equation (16)).
- Thermocouple temperature (Equation (20)).

They were solved in MATLAB (R2022a, MathWorks) using a stiff solver (ODE23S).

Table 2. Initial condition values used in simulation of time–temp profiles.

Property	Units	Value
Moisture, X_b	kg kg^{-1}	0.1006
Dimension a	mm	6.18
Dimension b	mm	3.84
Dimension c	mm	8.54
Equivalent Diameter, d_b	mm	5.87
Packing Density	kg^{-1}	10,224
Bean Temperature, T_b	°C	20

The inlet air and product temperatures were first extracted from the experimental data. Thermophysical properties of air were calculated using Equations (A6)–(A8). Airflow was determined based on constant fan frequency set-points using the prescribed calibration (Equations (A1) and (A2), respectively) and corrected due to temperature-dependent changes in air density. Both the temperature and airflow data (with a sample interval of 1 s) were interpolated using a smoothing spline (smoothing parameter 0.99) according to the solver's time span and step size.

The initial conditions for the batch mass and moisture content were specified as the measured green coffee properties (as in Table 2). The initial thermocouple temperature was the measured value at product loading during roasting trials (i.e., experimentally determined), whilst the initial 'actual' bean temperature was assumed equal to the ambient temperature (c. 20 °C). The number of beans in the batch was estimated from the initial batch mass and packing density—as noted in Table 2.

The coffee's transient thermophysical properties were estimated via the following empirical correlations; the goodness of fit of these correlations are detailed in Table 3.

Correlating density and moisture,

$$\rho_b = 8721 X_b + 422 \quad (21)$$

volume and moisture,

$$V_b = -1045X_b + 207 \tag{22}$$

thermal conductivity and density,

$$k_b = 7.31 \times 10^{-5}\rho_b + 0.045 \tag{23}$$

specific heat capacity and density,

$$C_{p,b} = 2.59 \times 10^{4}\rho_b^{-0.45} \tag{24}$$

Table 3. Correlation of physicochemical and thermophysical properties for coffee roasted under different airflow and batch size combinations in a spouted bed roaster—data is also visualised in Figure 7. Correlations for moisture applicable in the range of 1.1–6.9; for density in the range of 530–1047 kg m^{-3}.

Properties Correlated	Equation Number	R^2	RMSE
Density and moisture	(21)	0.9775	28 kg m^{-3}
Volume and moisture	(22)	0.9401	7.3 mm^3
Thermal conductivity and density	(23)	0.9779	0.002 W m^{-1} K^{-1}
Specific heat capacity and density	(24)	0.9704	27 J kg^{-1} K^{-1}

To simplify the implementation of volume expansion (back-calculated from the correlation of volume and moisture), a spherical bean geometry was assumed. Principal dimensions were used to estimate the equivalent-volume diameter (where the bean's equivalent diameter was determined based on its volume using Equation (3)), such that $d_b = (abc)^{1/3}$. In this way, the surface area of a coffee bean is thus

$$A_{s,b} \approx \pi d_b^2 \tag{25}$$

whereas the total area of the batch available for air-to-bean heat transfer is as follows:

$$A_{ab} \approx n_b A_{s,b} \tag{26}$$

Dimensionless numbers Re, Pr, Nu and Bi described the flow regime and thermal effectiveness associated with air-to-bean heat transfer. The Biot number, Bi, was employed initially to approximate the thermal inertia of the bean bed, in which convective heat transfer rates are lower relative to those expected in the spouting region [36,49,57]. These similarity parameters were designed to respond to the temperature-dependent properties of the drying air and transient physical properties of the coffee beans that evolve during roasting.

Endothermic cooling was determined based on the latent heat of vaporisation, i.e., according to Equation (A10) in Appendix A, where the water temperature was assumed equal to the simulated bean temperature.

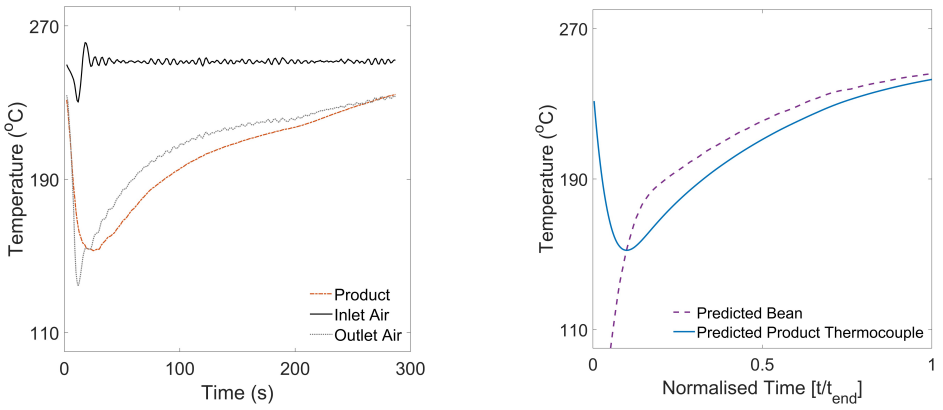
The kinetic models outlined in Equations (27) and (30) predicted changes in mass and moisture, respectively, whilst the drying air's temperature differential across the roaster was approximated as in Equation (17). The actual bean temperature was translated to the product (thermocouple) temperature via Equation (20) to account for the slow thermocouple response time and thus be compared with experimentally measured time–temperature profiles.

A non-linear least squares fitting procedure was implemented using a trust-region-reflective algorithm to estimate parameters η_A, K and Q_{am}, within specified constraints—the

estimation procedure is discussed in the next section. Initial guesses for the estimated parameters were random values between the specified constraints. The ODE solver's time span was specified as the time to first crack for each test case, with a step size of 0.1 s for all cases.

The simulation aimed to minimise the RMSE between the time–temperature profiles predicted via Equation (20) and those obtained experimentally—this temperature difference, Δ_T, was thus the cost function for the fitting procedure. The fitting procedure, based on gradient descent algorithms, assumed that a local minimum was found when the gradient of the cost function was $\leq 1 \times 10^{-7}$ and was performed three times (and checked for parameter convergence), with the estimated value from the first pass used as the initial guess for subsequent passes.

The time–temperature roasting profiles according to process conditions in Table 1 were simulated using the zero-dimensional, batch-scale model (Equations (16), (20), (27) and (30),)—RMSE was evaluated up to the onset of endo/exothermic reactions around first crack. An example of the experimental and predicted time–temperature profiles are displayed in Figure 4.



(**a**) Experimental (**b**) Predicted

Figure 4. Exemplar time–temperature roasting profiles illustrating (**a**) inlet air, outlet air and product thermocouple data collected experimentally and (**b**) thermocouple and bean temperatures predicted from the batch-scale simulation. Data corresponding to 350g batches roasted at 250 °C with a fan frequency of 48 Hz.

2.2.5. Validation of the Numerical Scheme

To validate the numerical scheme, the zero-dimensional model was modified to reflect the Schwartzberg [36] model, calibrated with their process and product properties and validated using experimental data presented therein. A comparison of experimental and predicted data is shown in Figure 5, with details of implementation, model parameters, product properties and initial conditions detailed in Appendix A.

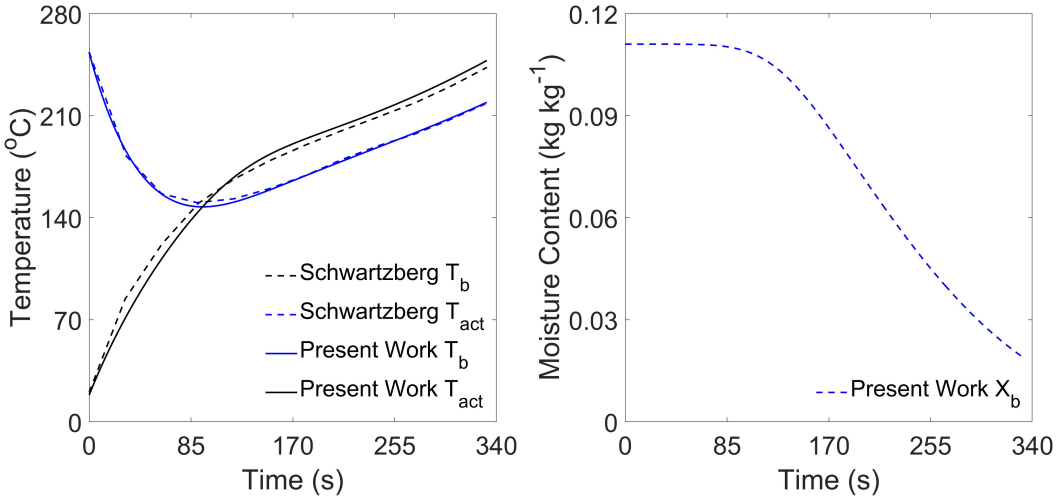


Figure 5. Validation of model against data published by Schwartzberg [36].

2.2.6. Determination of Model Parameter Bounds

Prior to calibration, the thermal model was queried to assess the sensitivity of the simulation (and the predicted time–temperature response) and to set the appropriate bounds for each of the parameters to be estimated: the thermal response coefficient (K in Equation (20)), the air-to-metal heat transfer (Q_{am} in Equation (16)) and the heat transfer effectiveness factor (η_A in Equation (18)).

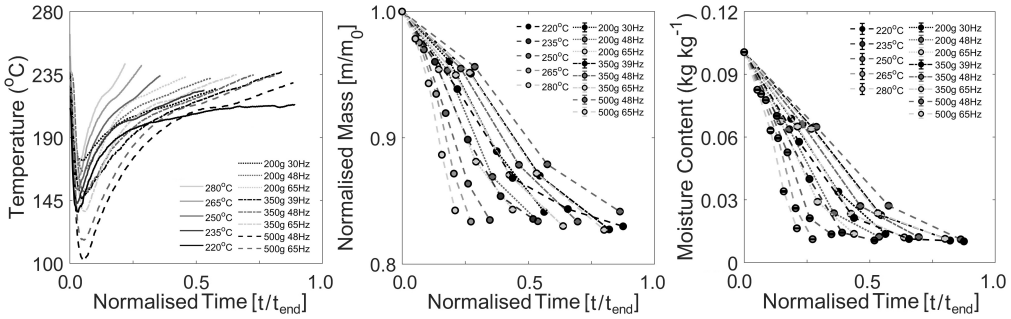
In the analysis detailed in (Appendix A.7), each of the parameters was varied and their effect on the predicted time–temperature profiles was plotted. For these simulations, a constant inlet air temperature of 250 °C, fan frequency of 48 Hz and a batch size of 0.35 kg was used. Based on these analyses, the air-to-metal heat transfer rate was assumed negligible (i.e., $Q_{am} = 0$ W) for the following simulations. The thermal response coefficient and the heat transfer effectiveness factor were estimated in the bounds of $0.01 \leq K \leq 1.00$ s^{-1} and $0.01 \leq \eta_A \leq 1.00$, respectively. Using the least squares fitting procedure (outlined in Section 2.2.4), η_A and K were estimated such that the RMSE between the predicted (thermocouple) and experimental time–temperature profiles was minimised up to first crack.

The confidence intervals associated with the estimated parameters were determined by explicitly calculating the Fisher Information Matrix (FIM) from the Jacobian matrix and Mean Square Error (MSE), taking the inverse of the FIM to compute the Variance Covariance Matrix (VCM) and then performing a Student t-distribution to scale the residuals using 95% confidence intervals.

3. Results

3.1. Changes in Temperature and Physicochemical Properties with Time

The experiments in Table 1 are the same as those studied in Al-Shemmeri et al. [30]. The experimental time–temperature, mass and moisture loss profiles for case studies I and II are displayed in Figure 6. These data are used in the next section to calibrate kinetic models of mass and moisture loss during roasting.



(**a**) Time–temperature profiles (**b**) Mass loss (**c**) Moisture loss

Figure 6. (**a**) Time–temperature profiles for all roasting conditions, with corresponding changes in (**b**) mass (w.b.) and (**c**) moisture during roasting—data corresponds to case studies (I) for different constant inlet air temperatures (220, 235, 250, 265 and 280 °C) and (II) different batch sizes (200, 350 and 500 g) and airflow rates (0.0141, 0.0185, 0.0228 and 0.0310 kg s^{-1} corresponding to fan frequencies of 30, 39, 48 and 65 Hz).

As discussed in Al-Shemmeri et al. [30] and seen in Figure 6, there is an early drop in thermocouple temperature due to the influx of beans and air at ambient temperature (ca. 20 °C). The thermocouple's measured temperature depends on (i) heat transfer from both the drying air and beans in the bean-bed and (ii) its location inside the roasting chamber. In spouted bed roasters, the product thermocouple is positioned to minimise the impact of airflow on temperature measurement, yet this is inherently unavoidable [41]. After the turning point, product temperature rises rapidly due to the high temperature differential between the drying air and beans. Provided the coffee's residence time in the roaster is sufficient, inlet air and product temperatures should converge, although due to heat loss and thermocouple positioning, this was not observed. For roasts with low thermal loads (i.e., those with low inlet air temperatures or a large batch size and low airflow), the rate of change in product temperature tends to zero, implicit of a pseudo-steady-state, whilst roasts with high thermal loads (i.e., those with high inlet air temperatures or a small batch sizes and high airflow), the rate of change of product temperature varies due to the initiation of endothermic and/or exothermic reactions [58].

During roasting, coffee's thermophysical properties evolve due to heat and mass transfer phenomena; dehydration drives porosity development, with coffee density decreasing due to both volumetric expansion and loss of organic matter. Thermophysical properties are therefore inherently related to density and moisture content [31,59–61]. These data were correlated with moisture and density to implement within the model. Figure 7 shows the fit to data for correlations between density, volume and moisture content and thermal conductivity and specific heat capacity with density. The fitting equations are given in Table 3—linear fitting was attempted first and was sufficient for all but the specific heat correlation.

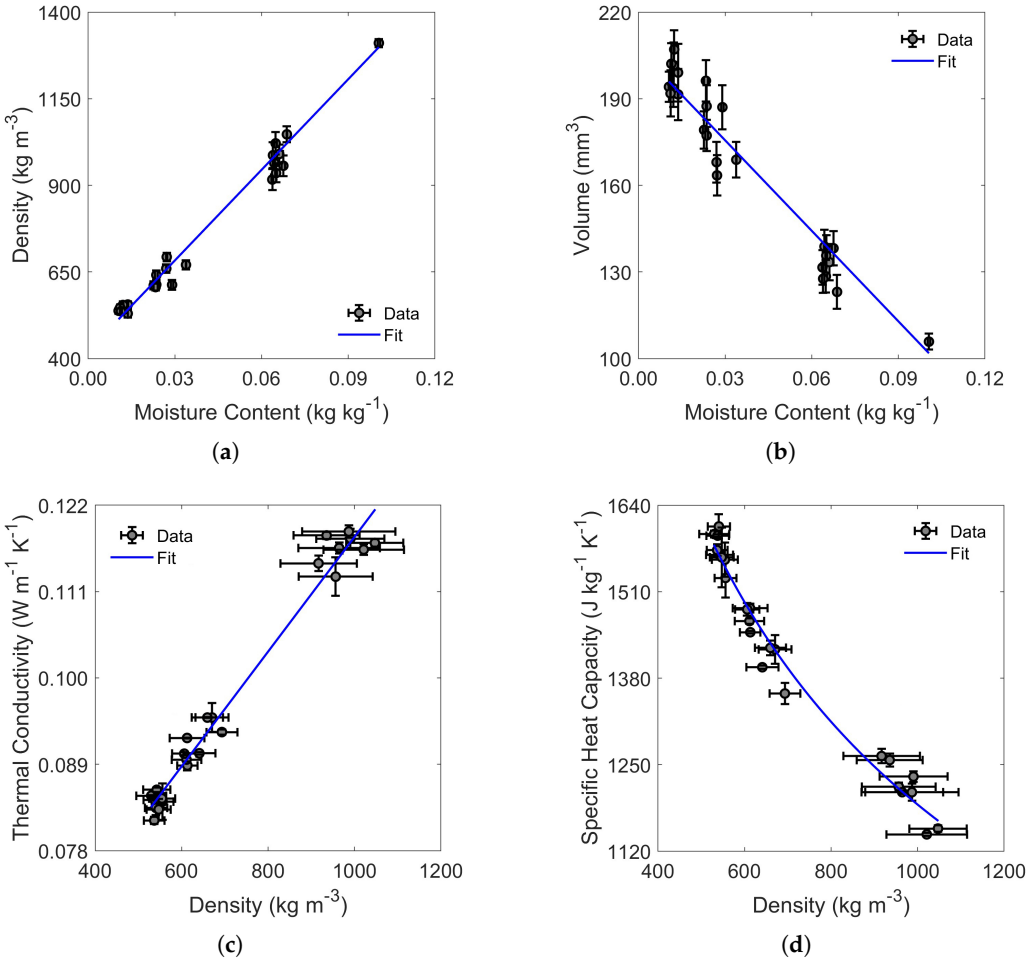


Figure 7. Correlations of (**a**) density and moisture, (**b**) volume and moisture, (**c**) thermal conductivity and density and (**d**) specific heat capacity and density for coffee roasted under different airflow and batch size combinations (specified in Table 1) in a spouted bed roaster.

Established relationships between these properties (Equations (21)–(24) in Table 3) were implemented as subroutines within the batch-scale simulations to account for coffee's transient properties.

3.2. Calibration of Kinetic Models of Mass and Moisture Loss

3.2.1. Mass Loss

For case studies I and II, first-order kinetics (i.e., $n = 1$ in Equation (8)) were used to predict mass loss during roasting.

For first-order kinetics, with an activation energy insensitive to process conditions, Equation (27) predicts coffee's mass loss during roasting with good accuracy at all roasting times and is robust to different constant inlet air temperatures (RMSE = 5.1 g) and different batch sizes and airflows (RMSE = 2.11 g). Parity plots are presented in Figure 8. To compare across batch sizes, data are presented as normalised mass loss (i.e., as a fraction of initial batch mass).

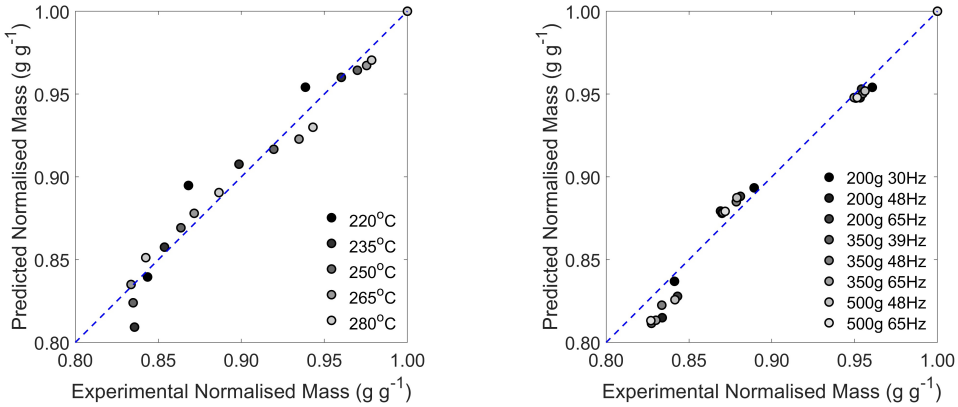
$$\frac{dm_{b,s}}{dt} = -k_{m_{b,s}} \exp\left(-\frac{656.8}{T_T}\right) m_{b,s} \tag{27}$$

The rate constant $k_{m_{b,s}}$ is plotted as a function of inlet air temperature in Figure 9a, which shows that higher constant inlet air temperatures increased the rate coefficient, hence for case study I, the rate coefficient, where $R^2 = 0.994$ is as follows:

$$k_{m_{b,s}} = 4.21 \times 10^{-5} T_{a,i} - 0.0192 \quad (28)$$

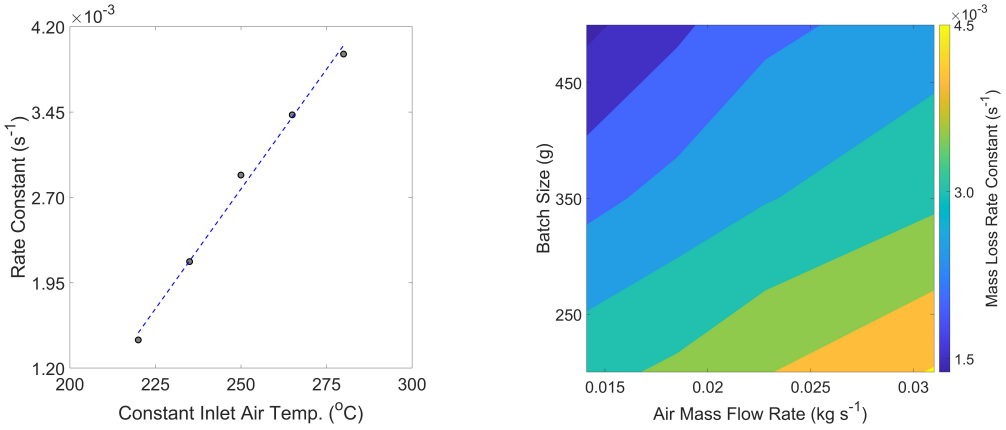
Figure 9b plots the rate constant as a function of airflow and batch size, and shows that high airflows and lower batch sizes correspond to greater mass loss rates, so for case study II, the rate coefficient, where $R^2 = 0.9732$, is as follows:

$$k_{m_{b,s}} = 3.59 \times 10^{-3} - 5.63 \times 10^{-3} m_{b,s,0} + 6.30 \times 10^{-2} G_a \quad (29)$$



(**a**) Case Study I (**b**) Case Study II

Figure 8. Comparison of predicted and experimental normalised mass loss profiles modelled using 1st-order kinetics (Equation (27)) for variation in (**a**) constant inlet air temperature (where rate constant, $k_{m_{b,s}}$, is calculated by Equation (28)) and (**b**) batch size and airflow (where $k_{m_{b,s}}$, is calculated using Equation (29))–data presented as parity plot.



(**a**) Case Study I (**b**) Case Study II

Figure 9. Impact of process conditions: (**a**) constant inlet air temperature (case study I) and (**b**) batch size and airflow (case study II) on the rate constant for 1st-order kinetic models of mass loss (Equation (27)).

Within the bounds of the experimental study, coupling Equations (27) with either (28) and (29) enable prediction of mass loss with good accuracy at all the roasting times.

3.2.2. Moisture Loss

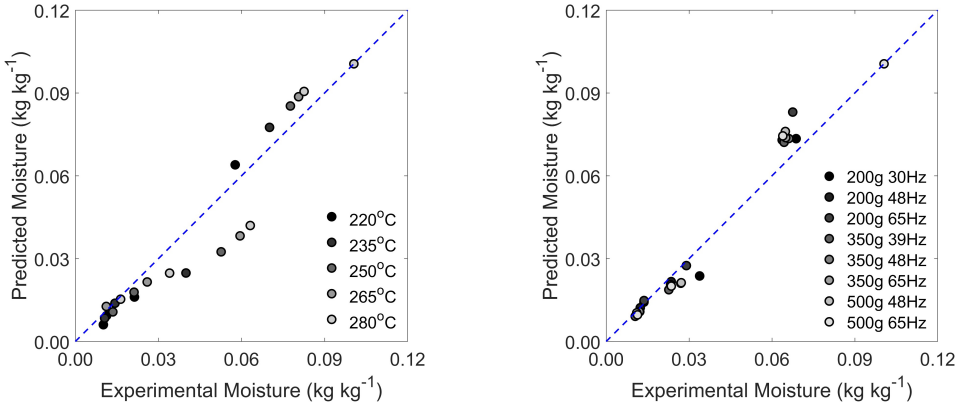
For case studies I and II, second-order kinetics (i.e., $n = 2$ in Equation (8)) were used to predict coffee's dehydration (i.e., change in moisture content) during roasting.

For second-order kinetics, with an activation energy insensitive to process conditions, Equation (30) predicts moisture loss with good accuracy at all the roasting times for both case study I (RMSE = 0.007 kg kg^{-1}) and II (RMSE = 0.005 kg kg^{-1}). Parity plots are presented in Figure 10 to compare the predicted and experimental moisture data.

$$\frac{dX_b}{dt} = -4.13 \times 10^6 \exp\left(-\frac{7908}{T_T}\right) X_b^2 \quad (30)$$

For both case studies, Equation (30) was found able to predict changes in moisture during roasting. Equation (30) predicts moisture content with good accuracy, although a greater sampling frequency would be beneficial to more accurately capture the early- and long-time behaviour during roasting.

For higher inlet temperatures, the goodness of fit was low midway through the roast—although the overall RMSE of the model is good, it probably does not capture all of the real physics and chemistry underway in the bean.



(**a**) Case Study I (**b**) Case Study II

Figure 10. Comparison of predicted and experimental moisture loss profiles modelled using 2nd-order kinetics (as in Equation (30)) for variation in (**a**) constant inlet air temperature (case study I) and (**b**) batch size and airflow (case study II)–data presented as parity plot.

3.3. Calibration of the Thermal Model

Data corresponding to the two case studies—i.e., (I) variation in constant inlet air temperature and (II) variation in batch size and airflow—were used here to calibrate the heat transfer simulations, wherein parameters K and η_A were estimated for each process condition. For each case study, comparisons of the experimental and predicted time–temperature profiles are presented, followed by correlations of the estimated parameters with process conditions.

3.3.1. Case Study I—Variation in Constant Inlet Air Temperature

Prediction of the time–temperature profiles corresponding to different constant inlet air temperatures on coffee's roasting transformation (at moderate batch size (0.35 kg) and airflow (48 Hz fan frequency)) was achieved with good accuracy prior to first crack. Comparisons of the predicted and experimental time–temperature profiles are presented in Figure 11.

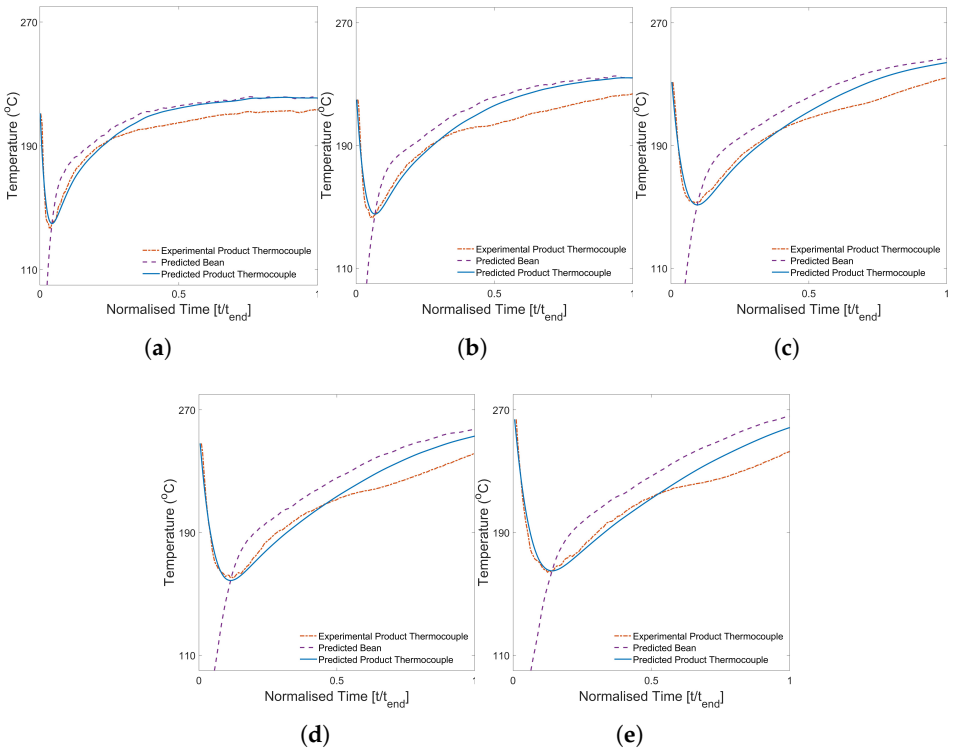


Figure 11. Predicted and experimental time–temperature roasting profiles corresponding to (**a**) 350 g 220 °C 48 Hz, (**b**) 350 g 235 °C 48 Hz, (**c**) 350 g 250 °C 48 Hz, (**d**) 350 g 265 °C 48 Hz and (**e**) 350 g 280 °C 48 Hz.

The predicted thermocouple time–temperature profiles agree well at early times, accurately capturing the response of the thermocouple and the 'turning point'. For the highest constant inlet air temperature condition (Figure 11e), the predicted profile begins to diverge from the experimental profile at approximately $t = 0.5t_{end}$, wherein the predicted profile overestimates the temperature. As the constant inlet air temperature decreases, the time at which divergence occurs decreases, such that for the lowest constant inlet air temperature condition (Figure 11a), divergence occurs at approximately $t = 0.25t_{end}$. The temperature difference observed in the later stages of roasting has previously been attributed to exothermic reactions [36], yet these data suggest that the washed-processed coffee used in these studies behaves differently. Particularly at high constant inlet air temperatures, there is an apparent plateau in the thermocouple temperature at around $t = 0.5t_{end}$ that is attributed to a decrease in the heating rate or possibly the effect of endothermic cooling.

Off-line (analytical) measurements of coffee's thermal degradation indicate that moisture is generated in the late stages of roasting due to Maillard-type reactions and pyrolysis [3,36]. Monitoring the levels of water and carbon dioxide in the exhaust of a roaster, Geiger [3] observed that even with the combined on- and off-line measurements, there is insufficient evidence to indicate that this alone is responsible for the reduced heating rate. The change in temperature response in the late stages of roasting could, therefore, be attributed to the cell wall's return to the glassy state [3], melting of galacto-mannans [3,62] or the generation of carbon dioxide [3] and carbon monoxide. It is expected that differences in coffee's cellular composition established during plant growth and cherry ripening and the extent of cellular degradation due to different post-harvest processing methods will determine both the cellular and chemical degradation during the softening and hardening phenomena that occur during roasting.

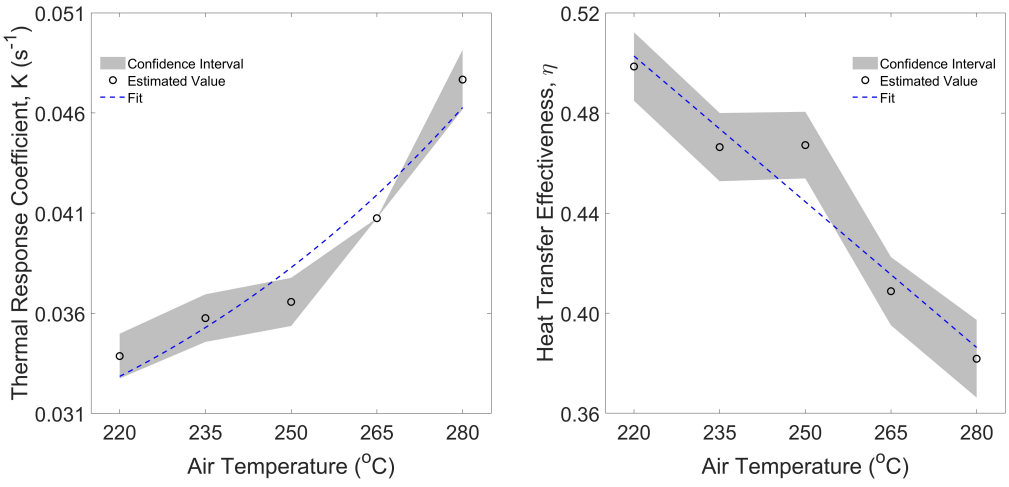
The estimated parameters and corresponding RMSE of the predicted time–temperature profiles are outlined in Table 4.

Table 4. Estimated parameters from the batch-scale, zero-dimensional simulation of time–temperature roasting profiles for the study of different constant inlet air temperatures.

Inlet Air Temp. (°C)	Batch Size (kg)	Fan Freq. (Hz)	Thermal Response Coefficient (s^{-1})	Effectiveness Factor	RMSE (°C)
220	0.35	48	0.034 ± 0.001	0.50 ± 0.01	4.4
235	0.35	48	0.036 ± 0.001	0.47 ± 0.01	4.7
250	0.35	48	0.037 ± 0.001	0.47 ± 0.01	4.9
265	0.35	48	0.041 ± 0.000	0.41 ± 0.01	4.3
280	0.35	48	0.048 ± 0.001	0.38 ± 0.02	5.1

There was no indication that the RMSE correlates with the input variable (constant inlet air temperature), so no systematic issues were apparent. Figure 12 presents a comparison of the estimated and predicted (from Equations (31)–(32)) parameter values for both the thermal response coefficient (Figure 12a) and heat transfer effectiveness factor (Figure 12b).

Figure 12a shows that the thermal response coefficient increased as the constant inlet air temperature increased, demonstrating that the applied constant inlet air temperature affected the time and temperature of the roasting profile's global minimum (i.e., the 'turning point'). In Figure 12b, the heat transfer effectiveness is shown to decrease as the applied constant inlet air temperature increases. Whilst the heat transfer effectiveness factor is not affected by airflow, a lower heat transfer effectiveness factor corresponds to a greater heat transfer coefficient as the Nusselt number approximation (Equation (19)) overestimates the convective heat transfer coefficient. Note that as $\eta_A \rightarrow 0$, $alpha \rightarrow h_{ab}$. Values of η_A are in the range determined by Schwartzberg [36] for spouted bed roasters of different scales.



(**a**) Thermal Response Coefficient (**b**) Heat Transfer Effectiveness

Figure 12. Correlation of estimated (**a**) thermal response coefficient and (**b**) heat transfer effectiveness factor with applied process conditions (i.e., constant inlet air temperature for case study II).

Both K and η_A were found to correlate with T_{ai} (R^2 = 0.876; RMSE = 0.001 s^{-1} and R^2 = 0.929; RMSE = 0.01, respectively):

$$K = 9.86 \times 10^{-13} T_{ai}^{4.22} + 0.0253 \quad (31)$$

$$\eta_A = -1.94 \times 10^{-3} T_{ai} + 0.930 \quad (32)$$

3.3.2. Case Study II—Variation in Batch Size and Airflow

The accuracy of the predicted time–temperature profiles corresponding to different batch sizes and airflows was reasonable for most process conditions (as indicated in Table 5). Comparisons of the predicted and experimental time–temperature profiles are presented in Figure 13.

Table 5. Estimated parameters from the batch-scale, zero-dimensional simulation of time–temperature roasting profiles for the study of different batch size and airflow combinations.

Inlet Air Temp. (°C)	Batch Size (kg)	Fan Freq. (Hz)	Thermal Response Coefficient (s^{-1})	Effectiveness Factor	RMSE (°C)
250	0.20	30	0.021 ± 0.002	0.25 ± 0.03	8.4
250	0.20	48	0.031 ± 0.001	0.28 ± 0.01	4.3
250	0.20	65	0.045 ± 0.002	0.31 ± 0.02	4.2
250	0.35	39	0.038 ± 0.002	0.52 ± 0.02	6.5
250	0.35	48	0.035 ± 0.002	0.46 ± 0.02	5.7
250	0.35	65	0.049 ± 0.002	0.48 ± 0.02	4.8
250	0.50	48	0.063 ± 0.002	0.90 ± 0.02	4.1
250	0.50	65	0.059 ± 0.001	0.77 ± 0.02	3.3

Predictions of time–temperature profiles corresponding to the variation in batch size and airflow outlined in Figure 13 were generally similar to those seen in case study I.

At early times, airflow has a significant effect on the thermocouple's response. It is of course critical to recall the batch size used in this study and the thermocouple's position in the roasting chamber. As both batch size and airflow produce different particle dynamics (as established by [49]), the bean–thermocouple and air–thermocouple interactions are expected to be dependent on the fraction of beans in the bean bed and the packing of beans around the thermocouple. Although the predicted time–temperature profiles are generally reasonably accurate, those for smaller batch sizes (0.2 kg) struggle to capture the response of the thermocouple, whilst the fit for larger batch sizes (>0.2 kg) is significantly better at early times.

When considering the poor fitting at early times with the lack of fit beyond first crack, it is clear that the simulations struggle at low batch sizes. This is most probably due to the small scale of the roaster, and in particular, the loose packing of beans around the thermocouple and the bias toward measurement of air temperature. For larger spouted bed and rotating drum roasters with greater batch sizes, this effect is expected to be lower and so scale-up of the simulations to larger roasters is anticipated to yield better results.

Although the time–temperature profiles corresponding to roasts of low batch size and/or low airflow combinations were less well predicted, this could be due to the bean bed dynamics that influence the bias of the thermocouple's measurement toward the temperature of either the air or beans. This measurement bias is a problem for the simulations, as they attempt to capture the thermophysical interactions of both the air and the beans with the thermocouple. This, in turn, reveals the limits of the simulations, which are robust for different batch sizes operated at moderate to high airflow, but do not fully capture the phenomena for low batch size and low airflow conditions.

The estimated parameters and corresponding RMSE of the predicted time–temperature profiles are outlined in Table 5.

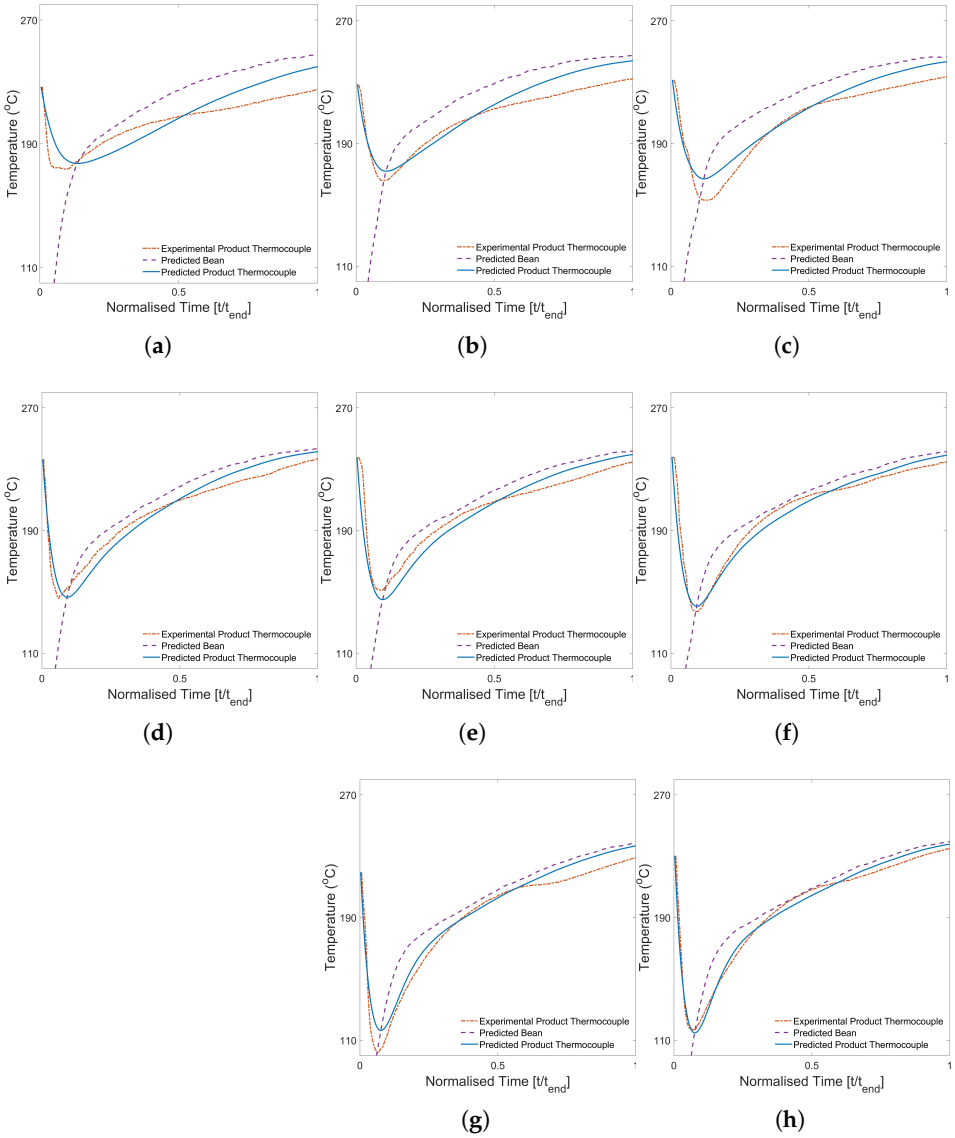


Figure 13. Predicted and experimental time–temperature roasting profiles corresponding to (**a**) 200 g 250 °C 30 Hz, (**b**) 200 g 250 °C 48 Hz, (**c**) 200 g 250 °C 65 Hz, (**d**) 350 g 250 °C 39 Hz, (**e**) 350 g 250 °C 48 Hz, (**f**) 350 g 250 °C 65 Hz, (**g**) 500 g 250 °C 48 Hz and (**h**) 500 g 250 °C 65 Hz.

The inclusion of the Biot number in Equation (18) reduces the heat transfer coefficient to account for the thermal inertia of the bean bed. The Nusselt number approximation (Equation (19)), therefore, overestimates the heat transfer coefficient. The heat transfer effectiveness was not significantly affected by airflow, suggesting that estimation of the heat transfer coefficient sufficiently accounts for variation in airflow due to its relation with Nusselt, Reynolds and Prandtl numbers (i.e., Equation (19)). Yet, this also suggests that the heat transfer effectiveness factor, in conjunction with the Biot number, is sufficient to account for variation in bean bed dynamics observed by Al-Shemmeri et al. [49]. Figure 14 presents a comparison of the estimated and predicted (from Equations (33) and (34)) parameter values for both the thermal response coefficient (Figure 14a) and heat transfer effectiveness factor (Figure 14b).

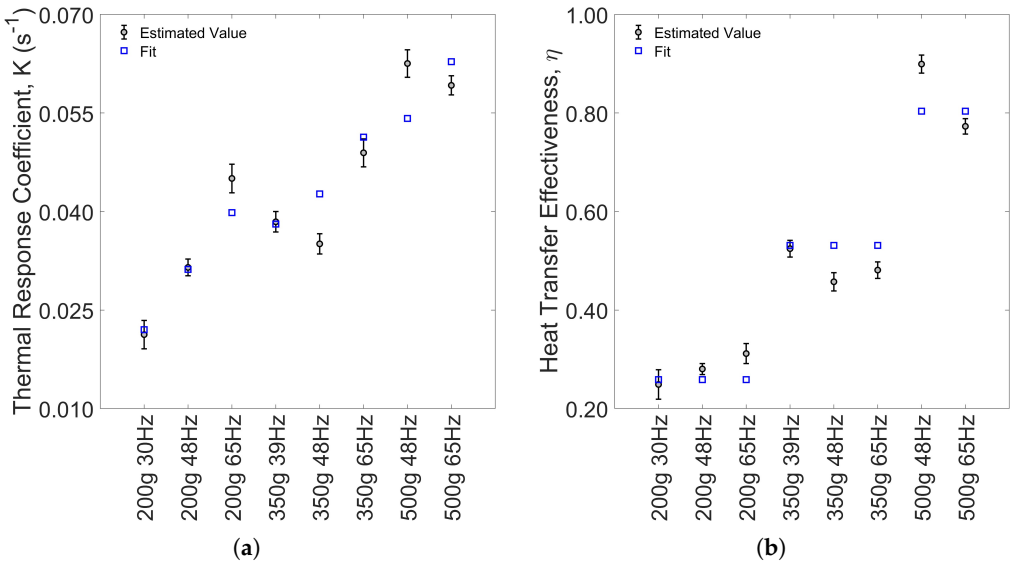


Figure 14. Correlation of estimated (**a**) thermal response coefficient and (**b**) heat transfer effectiveness factor with applied process conditions (i.e., batch size and airflow combinations).

Both the estimated parameters were found to correlate with the input variables. The thermal response coefficient, K, can be predicted based on air mass flow rate and batch size (R^2 = 0.873; RMSE = 0.006 s^{-1}):

$$K = -8.13 \times 10^{-3} + 1.05 G_a + 7.66 \times 10^{-2} m_{bs} \quad (33)$$

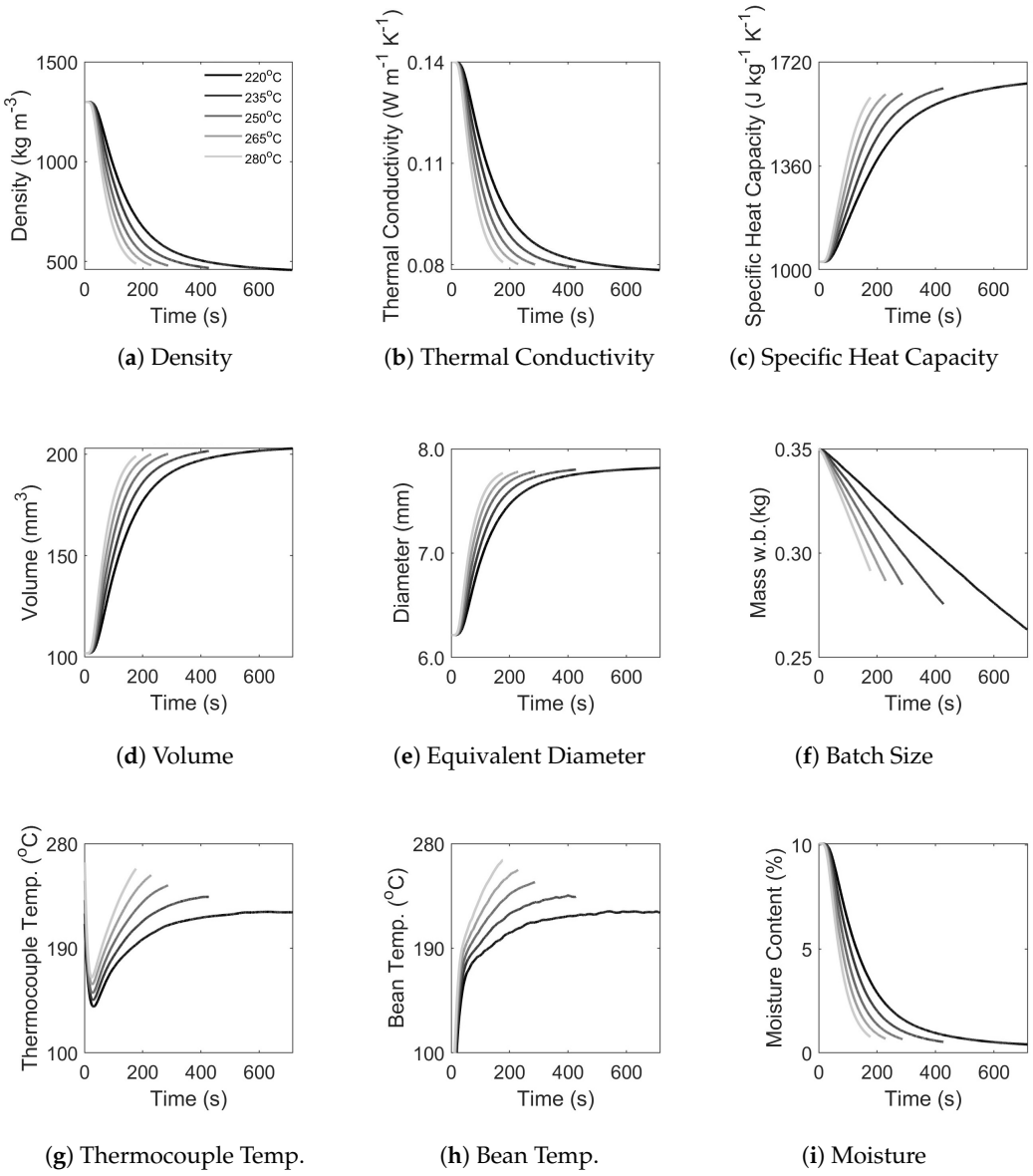
η_A can be predicted based on batch size (R^2 = 0.944; RMSE = 0.06):

$$\eta_A = 1.82 m_{bs} - 0.105 \quad (34)$$

3.4. Prediction of Coffee's Physicochemical Transformation

Predictions of the time–temperature profiles and coffee's corresponding physicochemical transformations for all the process conditions across the two case studies are made here using the calibrated simulations.

Figures 15 and 16 visualise the predicted time–temperature profiles and corresponding physicochemical transformations for simulations that replicated the two case studies used for calibration. These simulations utilise empirical measurements for the initial conditions of bean temperature, thermocouple temperature, batch size (mass basis) and moisture content from Tables 1 and 2. For both studies, the coffee's thermal properties, i.e., the density, thermal conductivity and specific heat capacity, are calculated via Equations (21), (23) and (24), respectively. The mass loss rate coefficient was calculated specifically for each study, i.e., using either Equation (29) for a constant inlet air temperature of 250 °C with different batch sizes and/or airflows or Equation (28) for different inlet air temperatures at constant batch size and airflow. Moisture loss kinetics (Equation (30)) were implemented for both studies. The thermal response coefficient and effectiveness factor were also calculated specifically for each study, such that Equations (33) and (34) were used for a constant inlet air temperature of 250 °C with different batch sizes and/or airflows, whereas Equations (31) and (32) were implemented for different inlet air temperatures at constant batch size and airflow. All the other methodologies are consistent across both case studies.



(**a**) Density (**b**) Thermal Conductivity (**c**) Specific Heat Capacity

(**d**) Volume (**e**) Equivalent Diameter (**f**) Batch Size

(**g**) Thermocouple Temp. (**h**) Bean Temp. (**i**) Moisture

Figure 15. Predicted time–temperature profiles and corresponding physicochemical development in coffee during simulated roasting at different constant inlet air temperatures. Subplots demonstrate the effect of process conditions on (**a**) density, (**b**) thermal conductivity, (**c**) specific heat capacity, (**d**) volume, (**e**) equivalent diameter, (**f**) batch size (mass basis), (**g**) thermocouple temperature, (**h**) bean temperature and (**i**) moisture. Data legend is displayed only in (**a**) for visual clarity.

Figures 15 and 16 present the simulated time–temperature profiles and coffee's physicochemical development, depicting simulations corresponding to different constant inlet air temperatures (200, 235, 250, 265, 280 °C) using a moderate batch size (0.35 kg) and moderate airflow (48 Hz fan frequency), i.e., case study I, in Figure 15, and different batch sizes (0.20–0.50 kg) and airflows (30–65 Hz fan frequency) using a moderate constant inlet air temperature (250 °C), i.e., case study II, in Figure 16. In both figures, the effect of process conditions on density, thermal conductivity, specific heat capacity, volume, equivalent diameter, batch size (mass basis), moisture, thermocouple temperature and bean temperature are illustrated.

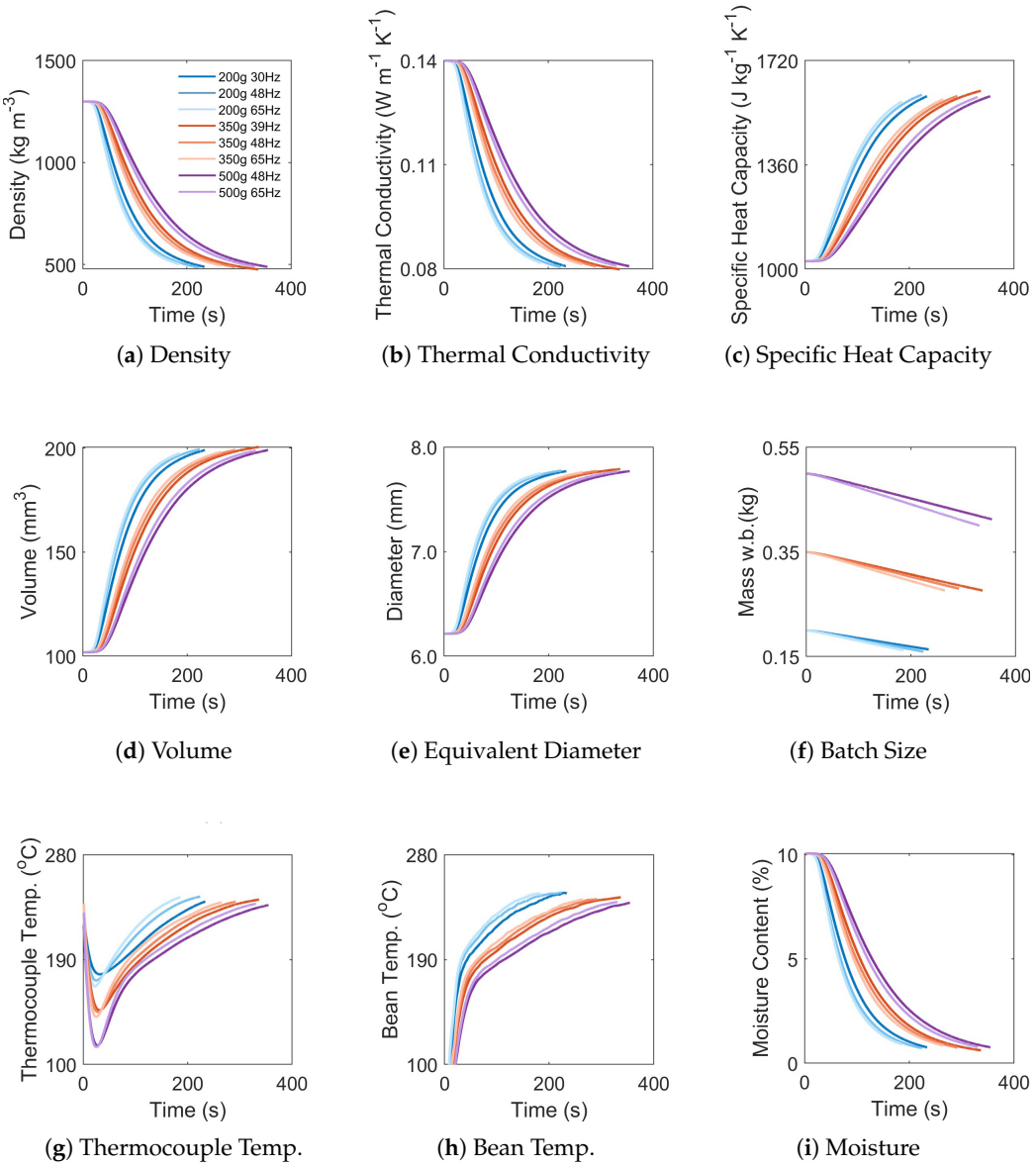


Figure 16. Predicted time–temperature profiles and corresponding physicochemical development in coffee during simulated roasting with different batch size and airflow combinations. Subplots demonstrate the effect of process conditions on (**a**) density, (**b**) thermal conductivity, (**c**) specific heat capacity, (**d**) volume, (**e**) equivalent diameter, (**f**) batch size (mass basis), (**g**) thermocouple temperature, (**h**) bean temperature and (**i**) moisture. Data legend is displayed only in (**a**) for visual clarity.

In Figure 15, greater constant inlet air temperatures correspond to higher thermal loads and, therefore, to a greater rate of change in bean and thermocouple temperature, greater mass and moisture loss and a more rapid volumetric expansion and density reduction. Regarding the predicted thermocouple temperatures, there is only a slight effect of constant inlet air temperature on the thermocouple's response (observed as the 'turning point'); yet, for times > 60 s, the temperature profiles deviate significantly with pseudo steady-state (and convergence with bean temperature) achieved around 500 s for all the conditions. The difference in pseudo steady-state temperatures correspond exactly to the difference in the applied constant inlet air temperature. These predicted phenomena are sensible and agree with the existing literature [1,46], yet temperature differentials observed across the roaster during preheating (i.e., heat loss) suggest that the predicted thermocouple temperature

should not converge with the inlet air temperature and is higher than expected during real roasting–also shown in Figure 4a.

Greater fan frequencies correspond to higher air mass flow rates and velocities. In Figure 16, airflow is shown to modulate heat transfer rates, affecting the heat transfer coefficient, thermal response coefficient and physicochemical development rates. Although the effect of airflow on moisture, bean size and density was less than was seen for different constant inlet air temperatures, mass loss was more sensitive. This indicates that airflow could be a powerful tool to modulate mass loss, whilst not greatly affecting bean size, moisture or density—at the pilot scale, this might also be attributed to bean/batch homogeneity.

Batch size determines the number of beans and the total surface area of the batch available for heat transfer. In these simulations, the number of beans scales based on the specified batch size and subsequently, the heat transfer area, A_{ab}, scales with it. The batch size also determines the bean bed mass fraction (as demonstrated by Al-Shemmeri et al. [49]), which affects the resulting thermal response coefficient and effectiveness factor. Batch size has a significant effect on all the predicted properties. Greater batch sizes correspond to lower rates of bean and thermocouple temperature evolution, which in turn reduces the rate of change of moisture, mass, bean size and density. The predicted profiles in Figure 16 show that at a given time, smaller batch sizes will have lower moisture and density, yet experimental data (presented in Appendix A) established that at the same colour, larger batch sizes, whose physicochemical transformation rates are lower, correspond to greater moisture and mass loss, and thus have lower roast yields.

Both Figures 15 and 16 demonstrate that all the input variables (constant inlet air temperature, batch size and airflow) have a significant effect on the simulated responses and their evolution rates. Changes in the volume, specific heat capacity, thermal conductivity and volume are estimated based on moisture kinetics; therefore, a higher rate of moisture loss corresponds to a more rapid (i) decrease in density and thermal conductivity and (ii) increase in volume and specific heat capacity. So if these responses were evaluated at a specified time, for example at $t = 100$ s, the physicochemical properties depend on the process conditions. Yet, if the same responses were evaluated at times that correspond to equivalent whole bean coffee colours that reflect realistic commercial products, the simulated (and experimental) findings indicate that some of these responses (moisture, volume and density) might be insensitive to process conditions.

4. Discussion

The discussion here is focused on the best practices for process and product developers in a commercial setting concerning coffee physicochemical properties, batch homogeneity and energy consumption.

4.1. Limitations and Robustness

The data-driven approach to this study provides novelty and enables well-calibrated simulations that accurately capture the real-system behaviour of coffee during roasting. The approach limits the applicability of the simulations when it comes to more diverse process conditions, different roaster designs and scales and different foodstuffs.

Kinetic models of mass loss were developed for each case study due to the sequential, compartmentalised approach to roasting exploration. This resulted in the need to implement "IF" functions that select the relevant subroutines used to determine the mass loss rate coefficient. This restricts the current simulation to specify either a different constant inlet air temperature or a different batch size and airflow combination. A larger study that follows a design of experiments approach and encompasses all input variables would

enable a global mass rate coefficient subroutine to be established and implemented in the simulation to model a broader range of roasting scenarios.

The correlation used here to include coffee volumetric expansion is relevant only for roasting and cannot account for (i) different initial bean sizes, (ii) swelling due to rehydration or (iii) shrinkage due to low temperature ($\leq$100 °C) drying. Development and implementation of a kinetic model to describe coffee's density and volumetric expansion would enable a greater range of scenarios to be queried, although inclusion of these models as ODEs can affect numerical stability during parameter estimation protocols.

Regarding generalisation of the model and applicability to other roasters, the energy balance is presented to demonstrate the governing equations, which intend to cover several roasting technologies. Calibrating the mass and moisture loss kinetics using bean temperature data reduces the need to understand the heat transfer effectiveness (i.e., transfer function from thermal input to beans). In this way, key data needed to translate these simulations to other roasters are the heat transfer coefficient(s) and thermal response coefficient. These will need to be tuned for each system given the significant differences in heat transfer mechanisms across design and scale. It is possible that implementation of particle motion data, defining coffee bean trajectories and assigning regional heat transfer coefficients—once validated—could enable these simulations to be used for more diverse roasting profiles.

Experimental studies of particle motion such as the ones by Al-Shemmeri et al. [49] for spouted bed roasters and Al-Shemmeri et al. [50] have been used to calibrate simulations as described in Che et al. [51]. These studies can be used to validate the arguments of Schwartzberg and derive design rules for regional heat transfer coefficients that enable generalisation of heat transfer equations.

After first crack, the predicted time–temperature profiles overestimated the batch-mean temperature. This significant deviation indicates that the thermodynamics of first crack do not correspond to sensible heating only and might be attributed to cellular degradation or latent heat.

4.2. Tools for Process and Product Development

Once parameters relating to characteristics of the roaster (thermal response coefficient) and applied process conditions (heat transfer effectiveness factor and heat loss across the roaster) are estimated for a range of process conditions, they can be fixed, reducing further need for process characterisation. The simulation, shown to be robust to different constant inlet air temperatures, batch sizes and airflows, thus enables the batch temperature, volume-averaged bean temperature, bean moisture content, batch mass, bean diameter, bean density and thermal properties to be predicted for known raw material properties and applied process conditions.

For application, developers can use the prescribed raw material properties and process parameters to explore the impact of batch size, constant inlet air temperature and airflow on coffee's time–temperature response. Furthermore, the prescribed process parameters can be used in conjunction with user provided coffee properties (different moisture contents, bean sizes and thermal properties) to explore their impact on final product properties.

5. Conclusions

Using a data-driven approach, a zero-dimensional, batch-scale simulation of coffee roasting time–temperature profiles was developed. Empirical characterisation of coffee's thermal and physicochemical journey from green to part-roasted and roasted enabled calibration of the simulation to predict real-system behaviour of coffee during roasting under a variety of process conditions.

Through measurements of airflow and temperature, the roaster's process parameters were calibrated and appropriately characterised to improve the accuracy and usability of the simulations. Correlations of coffee's physicochemical properties, used to determine the volumetric expansion, changes in density, specific heat capacity and thermal conductivity and kinetic models to describe changes in mass and moisture, were employed to inform coffee's physicochemical development during roasting. Dimensionless Reynolds, Prandtl and Nusselt numbers were used to approximate the heat transfer coefficient and used in conjunction with the bean-batch's surface area to estimate the heat flux.

Two estimated parameters were introduced to capture the characteristics of the roasting system that are not easily measured: the (i) thermal response coefficient and (ii) heat transfer effectiveness factor. Using a non-linear least squares fitting procedure (implemented as a trust-region-reflective algorithm), system-specific parameters were estimated and correlated with relevant input variables. These correlations were implemented as subroutines to include process-dependent parameters.

These simulations of heat and mass transfer during roasting provided accurate predictions of time–temperature profiles prior to first crack. The simulations were robust to variation in roasting process parameters including constant inlet air temperature, batch size and airflow, although the physics of real-system behaviour beyond first crack were not well captured. As many commercial control strategies decrease the thermal load as roasting progresses, comprehension of the observed deviations are necessary to improve the functionality of the simulations.

That said, this study demonstrated a robust tool for developers whose input variables are simple and rapid to measure and whose output provides predictions of coffee's time–temperature roasting profile and resulting physicochemical development. This work digitises process and product development procedures and therefore allows developers to virtually determine requirements for green coffee properties, process conditions or roasted coffee properties depending on their approach.

Author Contributions: M.A.-S.: writing—original draft, methodology, investigation, formal analysis, software, data curation and visualisation. P.J.F.: writing—review and editing, supervision, funding acquisition, conceptualisation and visualisation. R.F.: Writing—review and editing, supervision, funding acquisition and software. E.L.-Q.: writing—review and editing, supervision, formal analysis and software. All authors have read and agreed to the published version of the manuscript.

Funding: Authors acknowledge funding received from EPSRC through the Centre for Doctoral Training in Formulation Engineering (EngD studentship grant no. EP/L015153/1), and from JDE Peet's.

Institutional Review Board Statement: Not applicable.

Informed Consent Statement: Not applicable.

Data Availability Statement: The raw data supporting the conclusions of this article will be made available by the authors upon request.

Conflicts of Interest: Author Mark Al-Shemmeri is currently employed by the company JDE Peet's. He participated in conceptualisation, methodology, software, investigation and writing—original draft in the study. Author Robert Farr was employed by the company JDE Peet's. He participated in conceptualisation, methodology, investigation, resources, writing—review and editing, supervision, project administration and Funding acquisition in the study. The role of the company was providing resources—green coffee and roasting equipment for roasting and, tools and equipment for analysis. The remaining authors declare that the research was conducted in the absence of any commercial or financial relationships that could be construed as a potential conflict of interest.

Nomenclature

Definition	Term	Units
Time	t	s
Dimensionless property	Y	
Fan frequency	f	Hz
Mass loss	M_{loss}	%
Batch size	$m_{b,s}$	kg
Initial batch size	$m_{b,s,0}$	kg
Batch size (dry basis)	$m_{bs,db}$	kg
Principal dimensions	a, b, c	mm
Bean moisture	X_b	kg kg^{-1}
Bean diameter	d_b	m
Bean temperature	T_b	K
Actual bean temperature	$T_{b,a}$	K
Measured bean temperature	$T_{b,m}$	K
Bean volume	V_b	m^3
Bean surface area	$A_{s,b}$	m^2
Bean intrinsic density	ρ_b	kg m^{-3}
Bean individual mass	m_b	kg
Bean packing density	n_b	kg^{-1}
Bean bulk density	ρ_{bulk}	kg m^{-3}
Bean thermal diffusivity	D_b	mm^2 s^{-1}
Bean thermal conductivity	k_b	W m^{-1} K^{-1}
Bean specific heat capacity	$C_{p,b}$	J kg^{-1} K^{-1}
Air mass flow rate	G_a	kg s^{-1}
Air velocity	u_a	m s^{-1}
Inlet air temperature	$T_{a,i}$	K
Outlet air temperature	$T_{a,o}$	K
Air temperature	T_a	K
Air pressure	P_a	Pa
Air thermal conductivity	k_a	W m^{-1} K^{-1}
Air specific heat capacity	$C_{p,a}$	J kg^{-1} K^{-1}
Air viscosity	μ_a	Pa s
Air density	ρ_a	kg m^{-3}
Gas constant for air	R_a	J kg^{-1} K^{-1}
Overall air-to-bean heat transfer coefficient	α_{ab}	W m^{-2} K^{-1}
Air-to-bean heat transfer coefficient	h_{ab}	W m^{-2} K^{-1}
Air-to-bean heat transfer effectiveness factor	η_A	
Air-to-bean heat transfer area	A_{ab}	m^2
Bean-to-thermocouple heat transfer coefficient	h_{bt}	W m^{-2} K^{-1}
Bean-to-thermocouple heat transfer area	$A_{s,bt}$	m^2
Air-to-metal heat transfer coefficient	h_{am}	W m^{-2} K^{-1}
Air-to-metal heat transfer area	A_{am}	m^2
Metal surface temperature	T_m	K
Metal-to-bean heat transfer coefficient	h_{mb}	W m^{-2} K^{-1}
Metal-to-bean heat transfer area	A_{mb}	m^2
Latent heat of vaporisation of water	ΔH_v	J kg^{-1}
Latent heat of reaction	ΔH_r	J kg^{-1}
Nusselt number	$Nu = \frac{h_{ab} d_b}{k_a}$	
Reynolds number	$Re = \frac{d_b \rho_a u_a}{\mu_a}$	
Prandtl	$Pr = \frac{C_{p,a} \mu_a}{k_a}$	
Biot number	$Bi = \frac{h_{ab} d_b}{k_b}$	
Activation energy of property Y	E_a	J kg^{-1}

Reaction order index	n	
Thermocouple temperature	T_T	K
Thermal response coefficient	K	s^{-1}
Specific transfer rate into the beans	Q_b	W kg^{-1}
Specific transfer rate from air to beans	Q_{ab}	W kg^{-1}
Specific transfer rate from air to metal	Q_{am}	W kg^{-1}
Specific transfer rate from metal to beans	Q_{mb}	W kg^{-1}
Specific transfer rate of exothermic reactions	Q_r	W kg^{-1}
Specific transfer rate of endothermic reactions	Q_e	W kg^{-1}

Appendix A

Appendix A.1. Airflow Calibration

Many roasters use fan frequency for airflow set-points, yet conversion of these settings to velocity and mass flow rate (i.e., SI units) is required for implementation in heat and mass transfer models. For airflow calibration, both the air velocity and mass flow rate through the roaster were determined as a function of fan frequency using a hot-wire anemometer (405i, Testo) as described in [49]. Airflow calibrations for velocity (Equation (A1); R^2 = 0.999) and mass flow rate (Equation (A2); R^2 = 0.998) were thus

$$u_a = 0.165f - 0.71 \tag{A1}$$

$$G_a = 4.84 \times 10^{-4} f - 4.12 \times 10^{-4} \tag{A2}$$

Governing Equations

From steady-state, ambient temperature (c. 20 °C) airflow measurements, the velocity, u_a (m s^{-1}) and mass flow rate, G_a (kg s^{-1}), of air can be accurately estimated as a function of the fan setting f (Hz). The volumetric flow rate of air is a function of its velocity, u_a (m s^{-1}) and the cross-sectional area of the pipe, A_p (m^2) [63]:

$$V_a = u_a A_p \tag{A3}$$

The cross-sectional area of the pipe is a function of the pipe diameter, d_p (m) [63]:

$$A_p = \frac{\pi d_p^2}{4} \tag{A4}$$

where the measured equivalent pipe diameter for the pilot-scale spouted bed roasters was 60 mm. Assuming turbulent flow (where Re » 1) and that the mean air speed does not vary across the pipe, the air mass flow rate, G_a (kg s^{-1}), is a function of its density, ρ_a (kg m^{-3}) and volumetric flow rate, V_a (m^3 s^{-1}) [63]:

$$G_a = V_a \rho_a \tag{A5}$$

Data corresponding to the airflow calibration are presented in Figure A1.

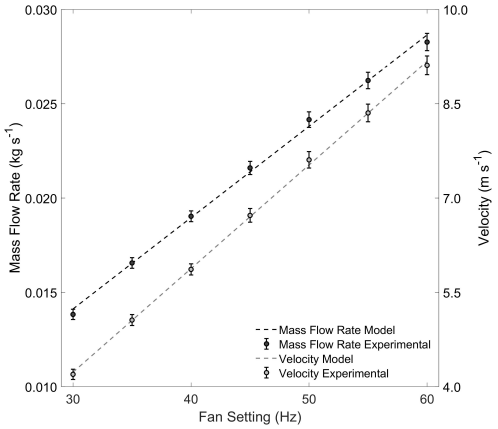


Figure A1. Correlation of velocity and air mass flow rate as a function of airflow setting for the pilot-scale spouted bed roaster—mass flow rate data correspond to the primary (left-hand) axis; velocity to the secondary (right-hand) axis.

Anemometer Installation

For the pilot-scale spouted bed roaster, the anemometer was installed on the air inlet, between the blower and heating element—for visualisation of installation, see Figure A2. The roaster was operated at ambient temperature (ca. 20–25 °C) with airflow settings varied between the minimum and maximum values of 30 and 65 Hz, respectively. Once steady-state conditions (i.e., constant airflows) were established, air velocity was measured for 5 min. Measurements were duplicated, with the mean and standard deviation of the velocities for each airflow setting calculated and subsequently used to determine inlet air mass flow rates.

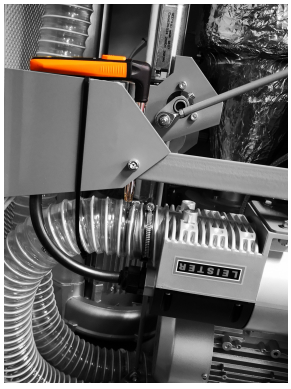


Figure A2. Installation of the hot wire anemometer (highlighted in colour) on the pilot-scale spouted bed roaster (desaturated for clarity) for airflow measurements.

During measurements in the spouted bed roasters, as the fan frequency increased, the measured temperature increased (ca. +19 °C)–likely due to dissipated heat from the fan's motor, surface friction between air and the fan's blades or pipe walls and intermolecular friction between air molecules (the latter only becomes significant under turbulent flow). As the air density is corrected according to the ideal gas law, roasters are typically operated above 200 °C and are often controlled to specified inlet air temperature; fan-induced heating is assumed negligible during roasting and not expected to impact experimental or model responses.

Appendix A.2. Thermophysical Properties of Air

Thermophysical properties of air depend on temperature and influence airflow through the roaster. Thermophysical data from Engineering-ToolBox were used to es-

timate the air's thermal conductivity, specific heat capacity and viscosity as a function of air temperature in the range of 0–300 °C. Air density was determined using the ideal gas law and the gas constant for air ($R_a = 287.05$ J kg^{-1} K^{-1}) [64], where roaster pressure was assumed atmospheric (101,325 Pa). The R-squared (R^2) (and Root Mean Squared Error (RMSE)) of models for thermal conductivity, specific heat capacity and viscosity were 0.9969 (6.0×10^{-4} W m^{-1} K^{-1}), 0.9979 (1.5 J kg^{-1} K^{-1}) and 0.9948 (4.4×10^{-7} Pa s), respectively.

$$k_a = 6.38 \times 10^{-5} T_a + 7.72 \times 10^{-3} \quad \text{(A6)}$$

$$C_{p,a} = 6.16 \times 10^{-5} T_a^{2.15} + 990 \quad \text{(A7)}$$

$$\mu_a = 3.61 \times 10^{-8} T_a + 8.1 \times 10^{-6} \quad \text{(A8)}$$

Air density was determined as a function of pressure and temperature [63]:

$$\rho_a = \frac{P_a}{R_a T_a} \quad \text{(A9)}$$

where the air temperature was that recorded by the anemometer.

The temperature-corrected air velocity can, therefore, be estimated via Equations (A1)–(A9).

Correlation of air's thermophysical properties with temperature, as described in Section 2.2.4, are displayed in Figure A3.

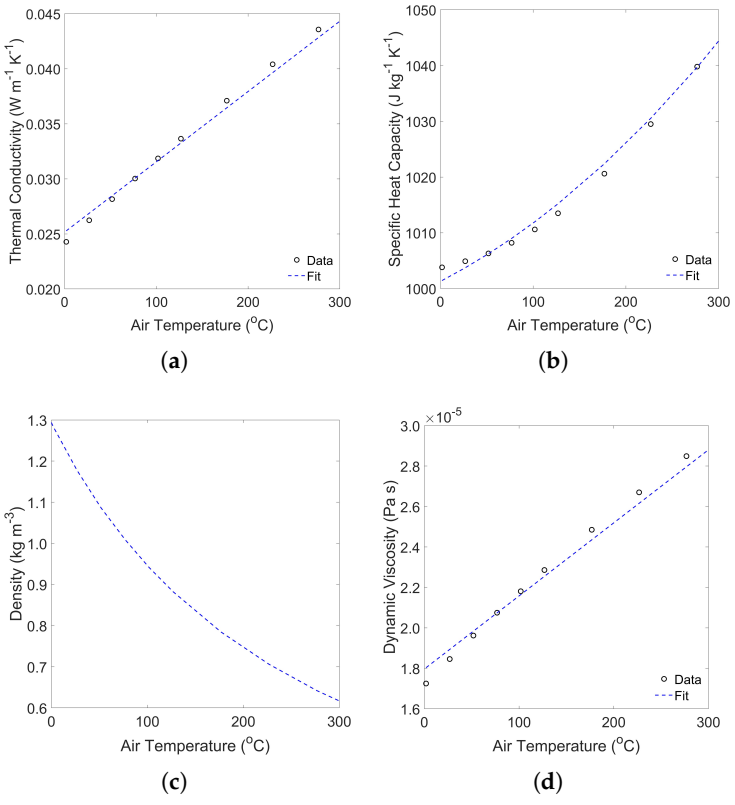


Figure A3. Correlation of air's thermal properties (**a**) thermal conductivity, (**b**) specific heat capacity, (**c**) density and (**d**) dynamic viscosity with air temperature.

Appendix A.3. Enthalpy of Vaporisation of Water

Data corresponding to the enthalpy of vaporisation of water at different temperatures [64] were fitted with a two-term exponential model (R^2 = 0.9937; $RMSE_{\Delta H_v, T_b}$ = 44.88 kJ kg^{-1}).

Water temperature was assumed equal to the mean bean temperature, with data applicable in the range of 0–300 °C.

$$\Delta H_v = -0.251 \exp(2.318 \times 10^{-2} T_b) + 2530 \exp(-1.268 \times 10^{-3} T_b) \quad \text{(A10)}$$

Appendix A.4. Comparison of Surface Area Approximation

From principal dimensions, volume, V_b (mm^3); surface area, $A_{s,b}$ (mm^2) and sphericity, ψ_b were calculated. Coffee geometry can be approximated to three geometries: (i) spherical, (ii) ellipsoidal and (iii) hemi-ellipsoidal. Modelled geometry is dependent on application. For most coffees, where $\psi_b \leq 0.8$, a hemi-ellipsoidal geometry is recommended; for high sphericity (peaberry) coffees, where $0.8 \leq \psi_b \leq 0.9$, an ellipsoidal geometry is more appropriate; for very high sphericity coffees where $\psi_b \geq 0.9$, a spherical geometry is appropriate.

For the spherical geometry, volume (V_b (mm^3)), surface area ($A_{s,b}$ (mm^2)) and sphericity (ψ_b) can be estimated as follows:

$$V_b = \frac{4\pi d^3}{3} \quad \text{(A11)}$$

$$A_{s,b} = \pi d^2 \quad \text{(A12)}$$

$$\psi_b = 1 \quad \text{(A13)}$$

For the ellipsoidal geometry, volume, surface area and sphericity can be estimated as follows:

$$V_b = \frac{4\pi (abc)^3}{3} \quad \text{(A14)}$$

$$A_{s,b} \approx 4\pi \left(\frac{(0.5ab)^{1.6} + (0.25ac)^{1.6} + (0.5bc)^{1.6}}{3} \right)^{\frac{1}{1.6}} \quad \text{(A15)}$$

$$\psi_b = \frac{(abc)^{(1/3)}}{a} \quad \text{(A16)}$$

For the hemi-ellipsoidal geometry, volume, surface area and sphericity can be estimated as follows:

$$V_b = \frac{4\pi (abc)^3}{6} \quad \text{(A17)}$$

$$A_{s,b} \approx 2\pi \left(\frac{(0.5ab)^{1.6} + (0.25ac)^{1.6} + (0.5bc)^{1.6}}{3} \right)^{\frac{1}{1.6}} + \frac{\pi ac}{4} \quad \text{(A18)}$$

$$\psi_b = \frac{(abc)^{(1/3)}}{a} \quad \text{(A19)}$$

Using these equations, the assumed geometry of the bean will determine the appropriate method to approximate the bean's surface area. For the Kenyan Arabica coffee used in these studies, the impact of the selected geometry on the approximated surface area was determined. The effect of scale was also assessed by considering beans using geometrical scaling factors of 0.5–2.0. Figure A4 displays the effect.

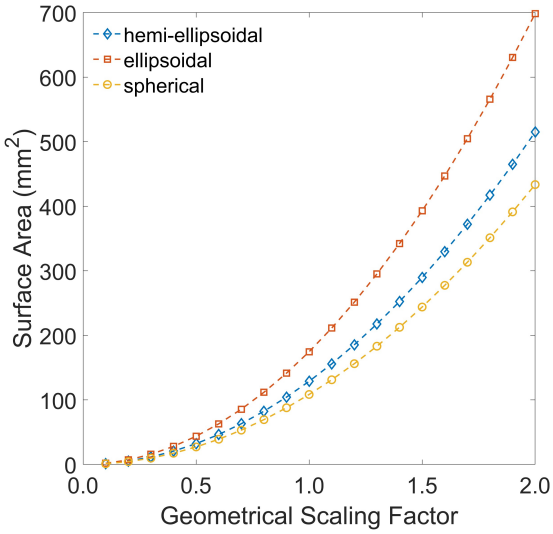


Figure A4. The effect of geometry selection and scale on the approximated surface area of a coffee bean.

Appendix A.5. Modelling Coffee's Physicochemical Transformation

Appendix A.5.1. Mass Loss

Figures A5 and A6 present a comparison of predicted and experimental mass loss data, for case studies I (variation in constant inlet air temperature) and II (variation in batch size and airflow), respectively. To compare across batch sizes, data in Figure A6 are presented as normalised mass loss (i.e., as a fraction of initial batch mass).

Appendix A.5.2. Moisture Loss

Figures A7 and A8 present a comparison of predicted and experimental moisture loss data for case studies I (variation in constant inlet air temperature) and II (variation in batch size and airflow), respectively.

Appendix A.6. Validation of the Model's Numerical Scheme

For implementation of the model, roast time was specified as 332 s and constant inlet air temperature as 482 °C. Air mass flow rate varies with thermocouple temperature, T_T, such that for $T_T \leq 182$ °C, $G_0 = 43$ kg s^{-1}, when $182 \leq T_T \leq 199$ °C, $G = 0.89G_0$ and when $T_T \geq 199$ °C, $G = 0.78G_0$. The heat transfer effectiveness factor was specified as 0.3. Air-to-bean heat transfer area was specified as 48 m^2. Although air mass flow rate varies with time, there was insufficient data to define a correlation between air velocity and air mass flow rate, so air velocity was set to be constant at 4 m s^{-1} [43].

Air thermal conductivity, specific heat capacity, air density and dynamic viscosity were constant, with values extracted from Engineering-ToolBox [64]: 4.04×10^{-2} W m^{-1} K^{-1}, 1029.5 J kg^{-1} K^{-1}, 0.4567 kg m^{-3}, 2.67×10^{-5} kg m^{-1} s^{-1}. Bean diameter was 6 mm and initial moisture content 0.111 kg kg^{-1}. The bean's thermal conductivity, k_b, and specific heat capacity, $C_{p,b}$, were a function of moisture content, X_b ($k_b = 0.356 + 0.139X_b$; $C_{p,b} = (1099 + 7T_b + 5000X_b)/(1 + X_b)$) [43]. Initial bean temperature was 18.3 °C, batch size 400 kg and dry matter mass assumed constant. Heat generation from exothermic reactions was a function of an apparent activation energy ($dQ_r/dt = Aexp(-E_a/RT_b)((H_{et} - H_e)/H_{et})$) where A = 116,200 kJ kg^{-1}, $-E_a/R$ = 5500 K, H_{et} = 232 kJ kg^{-1} and initial heat generation is zero, i.e., H_e = 0 kJ kg^{-1}. Latent heat of vaporisaiton was ΔH_v = 2790 kJ kg^{-1} and the moisture loss was a kinetic model ($dX/dt = (4.3210^9X^2)/d^2exp((-9889)/(T_b + 273.15))$). Bean temperature was a function of the thermocouple temperature ($(dT_T)/dt = K(T_b - T_T)$), where K = 0.013 s^{-1}. Initial thermocouple temperature was 253 °C.

Reasonable agreement between the predicted and experimental time–temperature profile is shown in Figure 5. Therefore, the numerical scheme and implemented model is sensible.

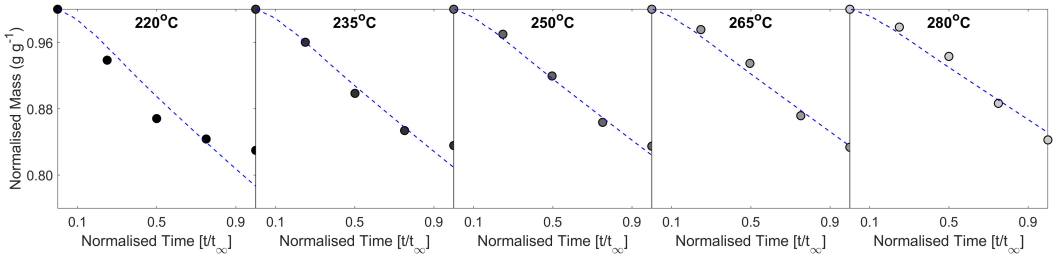


Figure A5. Comparison of the predicted and experimental data for 1st-order kinetic models of mass loss for the constant inlet air temperature study—data presented as kinetic time-series.

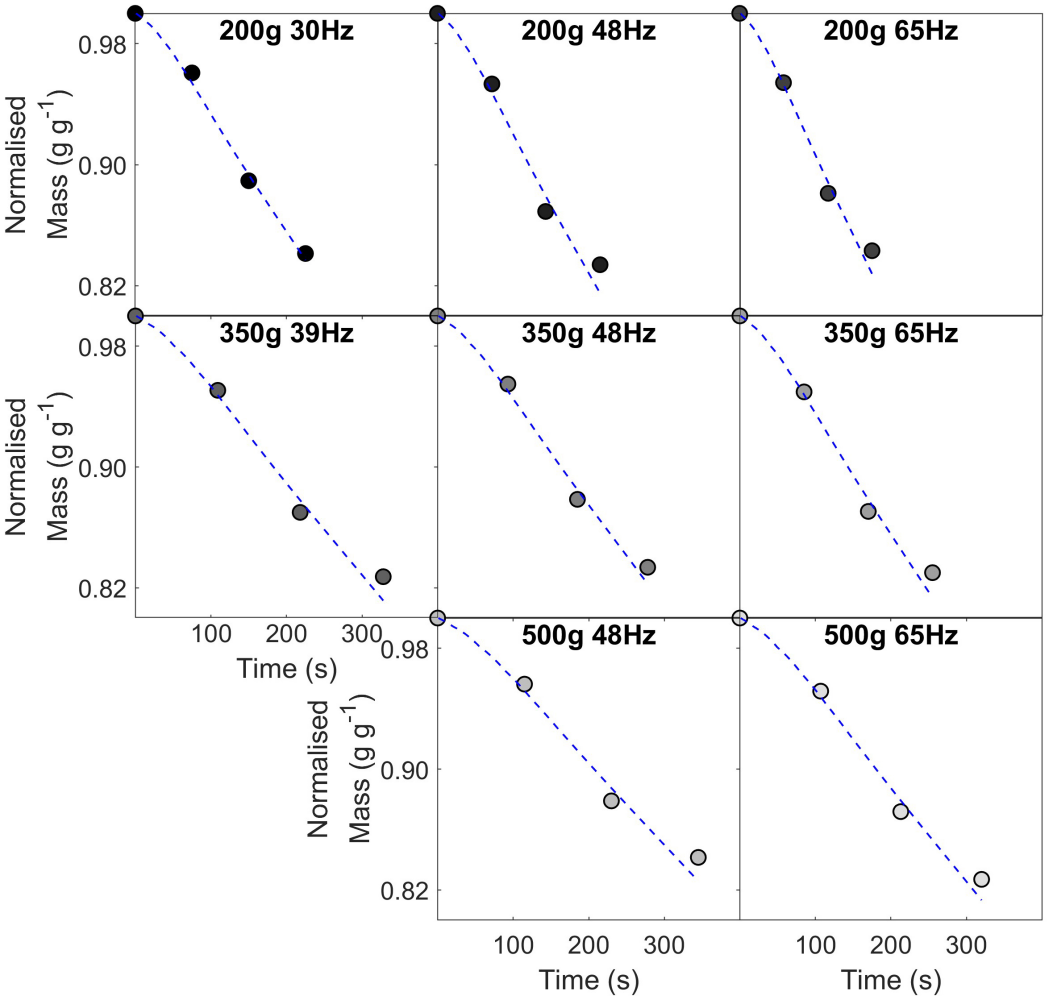


Figure A6. Comparison of the predicted and experimental normalised mass loss profiles modelled using 1st-order kinetics for the variation in batch size and airflow study—data presented as kinetic time-series.

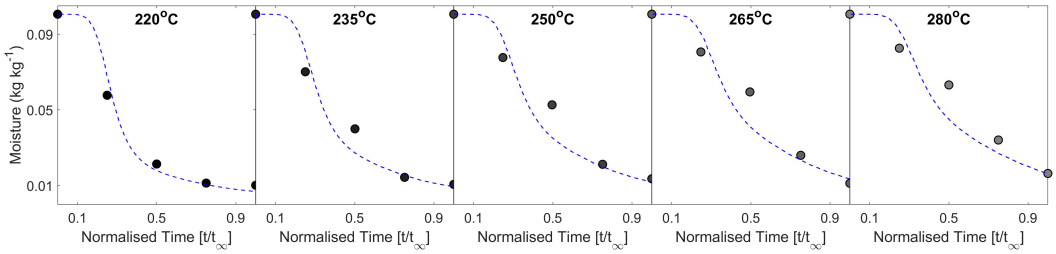


Figure A7. Comparison of the predicted and experimental data for 2nd-order kinetic models of moisture loss for the constant inlet air temperature study—data presented as kinetic time-series.

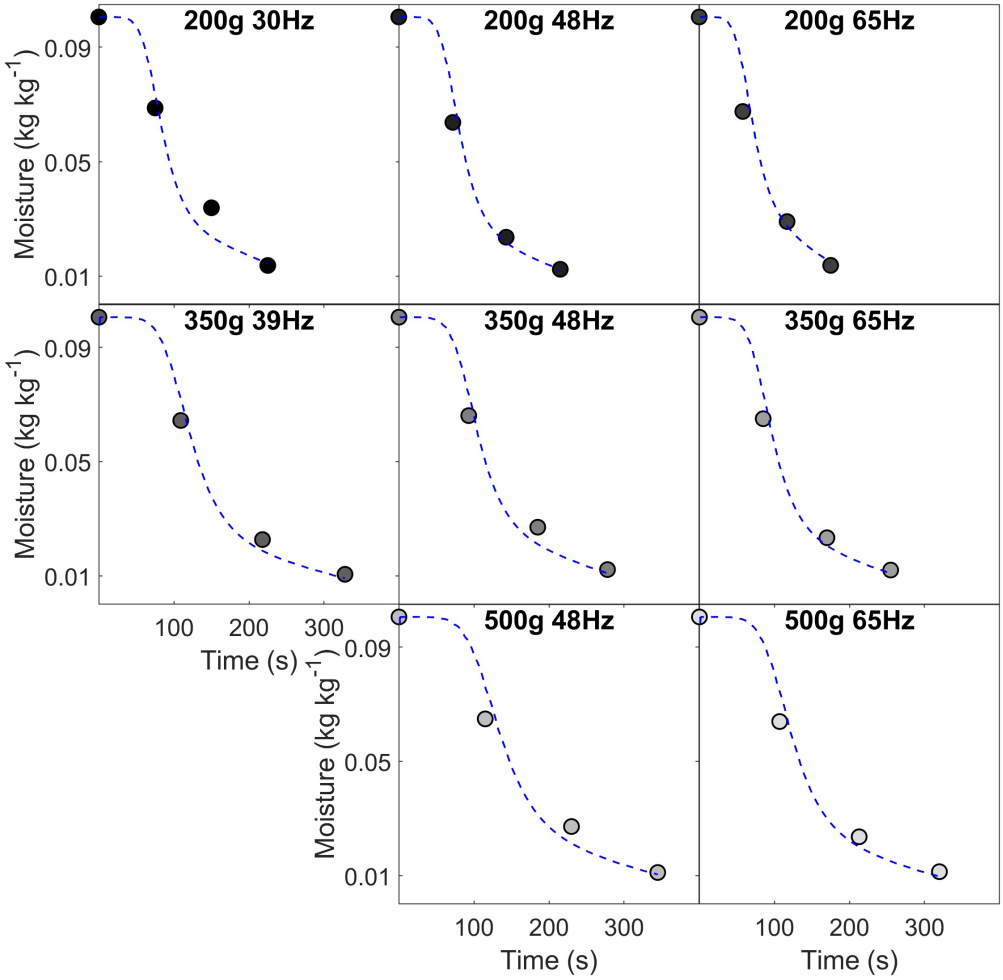


Figure A8. Comparison of the predicted and experimental moisture loss profiles modelled using 2nd-order kinetics for the variation in batch size and airflow study—data presented as kinetic time-series.

Appendix A.7. Determination of Model Parameter Bounds

This subsection aims to identify the sensitivity of the simulation (and the predicted time–temperature response) to variation in each of the estimated parameters–the thermal response coefficient (K in Equation (20)), the air-to-metal heat transfer (Q_{am} in Equation (16)) and the heat transfer effectiveness factor (η_A in Equation (18)). From these analyses, a feasible range of parameter values can be used to define the constraints of the parameters during estimation.

Appendix A.7.1. Thermal Response Coefficient

The thermal response coefficient was varied in the range of 0.01–1 s^{-1}, whilst air-to-metal heat transfer was assumed negligible (i.e., $Q_{am} = 0$) and the heat transfer effectiveness

factor was specified as 0.5. Figure A9 illustrates the effect of different thermal response coefficients on the predicted time–temperature response.

As the thermal response coefficient, K, increases, the thermocouple's response time decreases, thus reducing the time and temperature of the 'turning point' (the time–temperature profile's global minimum). The difference between the predicted temperatures of the thermocouple and the bean (T_T and T_b in Figure A9, respectively), which can be considered as the RMSE if T_b is the reference, decreases as K increases. Therefore, for thermocouples with higher values of K (i.e., with smaller diameters), the response is more rapid and accurate, relative to the predicted bean temperature—so as $1/K \to 0, T_T \to T_b$. The effect of airflow, bean bed dynamics and the temperature within the roasting chamber on the thermal response coefficient is sensible, as all of these will influence heat transfer rates from the system (i.e., the beans and the air) to the thermocouple. Conversely, this shows that for large diameter thermocouples with low values of K, the temperature measured by the thermocouple is expected to be delayed relative to the 'thermal reality' of the system.

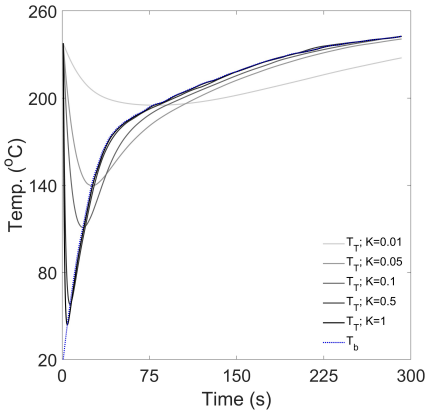


Figure A9. Sensitivity analysis to show the effect of thermal response coefficient, K, on the predicted time–temperature profile.

Appendix A.7.2. Air-to-Metal Heat Transfer

The air-to-metal heat transfer rate was varied in the range of 0–1500 W, whilst the thermal response coefficient was specified as 0.1 s^{-1} and the heat transfer effectiveness factor was specified as 0.5. Figure A10 illustrates the effect of different air-to-metal heat transfer rates on the predicted time–temperature response.

The air-to-metal heat transfer rate, Q_{am}, was introduced to account for heat loss across the system, which was observed as a difference between the measured inlet, product and outlet thermocouple temperatures (ca. 30 °C) at pseudo steady-state during preheating. Figure A10 shows that when Q_{am} is high, a pseudo steady-state is achieved during roasting, whereby the rate of change of temperature approaches zero. As Q_{am} decreases, the time and temperature to achieve the pseudo steady-state increases. These effects can be likened to a decrease in the applied thermal load, (i.e., a lower constant inlet air temperature) or reduced heat transfer efficacy. Therefore, Q_{am} is expected to correlate with the constant inlet air temperature and heat transfer effectiveness factor, which implies collinearity can be expected of the estimated parameters. For this reason, the air-to-metal heat transfer rate will be assumed negligible (i.e., $Q_{am} = 0$) for the time–temperature profile simulations, so that these effects are lumped into the heat transfer effectiveness factor to prevent collinear parameters, which could reduce their accuracy and robustness.

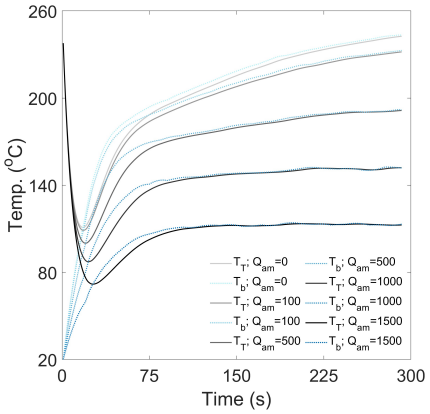
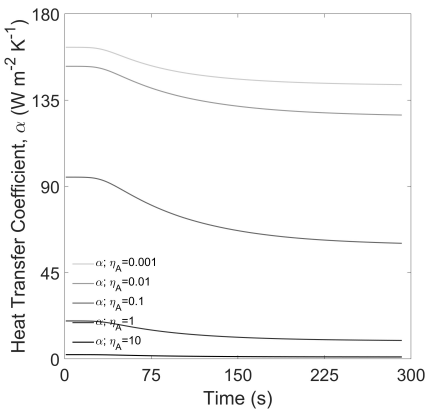


Figure A10. Sensitivity analysis to show the effect of air-to-metal heat transfer rate, Q_{am}, on the predicted time–temperature profile.

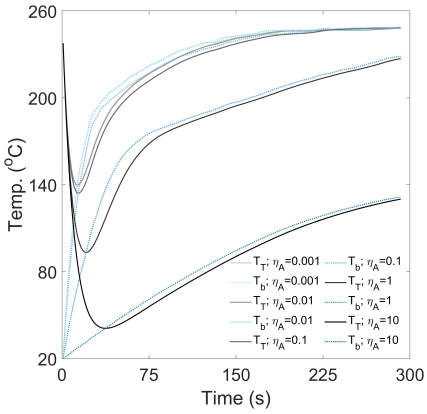
Appendix A.7.3. Heat Transfer Effectiveness

The heat transfer effectiveness factor was varied in the range of 0.001–10, whilst the thermal response coefficient was specified as 0.1 s^{-1} and the air-to-metal heat transfer was assumed negligible (i.e., $Q_{am} = 0$). Figure A11 illustrates the effect of different heat transfer effectiveness factors on both the heat transfer coefficient and predicted time–temperature response.

The heat transfer effectiveness factor, η_A, aims to account for heat loss across the system (such as air-to-metal heat transfer), as well as the availability of the coffee's surface area (both on the bean and batch scales). When roasting under flow regimes that produce large bean beds (i.e., those with a large batch size and low airflow, as demonstrated by Al-Shemmeri et al. [49]), the bean bed mass fraction (BBMF) is high and η_A is expected to be high due to the reduced airflow and lower convective heat transfer in the bean bed. When roasting under flow regimes that minimise the bean bed (i.e., those with a small batch size and high airflow), beans are in a constant recirculating motion and the convective heat transfer is greater—in this scenario, η_A is expected to be low. These effects are clearly depicted in Figure A11, whereby low values of η_A correspond to large heat transfer coefficients (Figure A11a) and rapid time–temperature responses (Figure A11b).



(**a**) Heat Transfer Coefficient



(**b**) Temperature

Figure A11. Sensitivity analysis to show the effect of air-to-metal heat transfer rate, Q_{am}, on the predicted time–temperature profile.

References

1. Heyd, B.; Broyart, B.; Hernandez, J.A.; Valdovinos-Tijerino, B.; Trystram, G. Physical Model of Heat and Mass Transfer in a Spouted Bed Coffee Roaster. *Dry. Technol.* **2007**, *25*, 1243–1248. [CrossRef]
2. Wang, N. Physicochemical Changes of Coffee Beans During Roasting. Ph.D. Thesis, University of Guelph, Guelph, ON, Canada, 2012.
3. Geiger, R. Development of Coffee Bean Structure During Roasting–Investigations on Resistance and Driving Forces. Ph.D. Thesis, ETH Zurich, Zurich, Switzerland, 2004. [CrossRef]
4. Rao, S. *The Coffee Roaster's Companion*; Scott Rao: Boulder, CO, USA, 2014.
5. Anokye-Bempah, L.; Styczynski, T.; de Andrade Teixeira Fernandes, N.; Gervay-Hague, J.; Ristenpart, W.D.; Donis-González, I.R. The effect of roast profiles on the dynamics of titratable acidity during coffee roasting. *Sci. Rep.* **2024**, *14*, 8237. [CrossRef] [PubMed]
6. Obando, A.M.; Figueroa, J.G. Effect of Roasting Level on the Development of Key Aroma-Active Compounds in Coffee. *Molecules* **2024**, *29*, 4723. [CrossRef] [PubMed]
7. Perrone, D.; Donangelo, R.; Donangelo, C.M.; Farah, A. Modeling Weight Loss and Chlorogenic Acids Content in Coffee during Roasting. *J. Agric. Food Chem.* **2010**, *58*, 12238–12243. [CrossRef]
8. Wang, X.; Lim, L.T. Investigation of CO2 precursors in roasted coffee. *Food Chem.* **2017**, *219*, 185–192. [CrossRef]
9. Baggenstoss, J. Coffee Roasting and Quenching Technology–Formation and Stability of Aroma Compounds. Ph.D. Thesis, ETH Zurich, Zurich, Switzerland, 2008. [CrossRef]
10. Bustos-Vanegas, J.; Correa, P.; Martins, M.; Baptestini, F.; Campos, R.; Horta de Oliveira, G.; Nunes, E. Developing predictive models for determining physical properties of coffee beans during the roasting process. *Ind. Crops Prod.* **2018**, *112*, 839–845. [CrossRef]
11. Marek, G.; Dobrzański, B.; Oniszczuk, T.; Combrzyński, M.; Ćwikła, D.; Rusinek, R. Detection and Differentiation of Volatile Compound Profiles in Roasted Coffee Arabica Beans from Different Countries Using an Electronic Nose and GC-MS. *Sensors* **2020**, *20*, 2124. [CrossRef]
12. Gancarz, M.; Dobrzański, B.; Malaga-Toboła, U.; Tabor, S.; Combrzyński, M.; Ćwikła, D.; Strobel, W.R.; Oniszczuk, A.; Karami, H.; Darvishi, Y.; et al. Impact of Coffee Bean Roasting on the Content of Pyridines Determined by Analysis of Volatile Organic Compounds. *Molecules* **2022**, *27*, 1559. [CrossRef]
13. Várady, M.; Tauchen, J.; Fraňková, A.; Klouček, P.; Popelka, P. Effect of method of processing specialty coffee beans (natural, washed, honey, fermentation, maceration) on bioactive and volatile compounds. *LWT* **2022**, *172*, 114245. [CrossRef]
14. Febrianto, N.A.; Zhu, F. Coffee bean processing: Emerging methods and their effects on chemical, biological and sensory properties. *Food Chem.* **2023**, *412*, 135489. [CrossRef] [PubMed]
15. Santanatoglia, A.; Alessandroni, L.; Fioretti, L.; Sagratini, G.; Vittori, S.; Maggi, F.; Caprioli, G. Discrimination of Filter Coffee Extraction Methods of a Medium Roasted Specialty Coffee Based on Volatile Profiles and Sensorial Traits. *Foods* **2023**, *12*, 3199. [CrossRef]
16. Louzada Pereira, L.; Rizzo Moreira, T. Quality Determinants in Coffee Production; Springer: Berlin/Heidelberg, Germany, 2021.
17. Seninde, D.R.; Chambers, E. Coffee Flavor: A Review. *Beverages* **2020**, *6*, 44. [CrossRef]
18. Tsiafitsa, A.; Oikonomopoulou, V.; Stramarkou, M.; Krokida, M.; Papassiopi, N. Effect of heat treatment on physicochemical and sensory properties of selected coffee varieties. *Eur. Food Res. Technol.* **2022**, *248*, 2009–2020. [CrossRef]
19. Dutra, E.R.; Oliveira, L.S.; Franca, A.S.; Ferraz, V.P.; Afonso, R.J.C.F. A preliminary study on the feasibility of using the composition of coffee roasting exhaust gas for the determination of the degree of roast. *J. Food Eng.* **2001**, *47*, 241–246. [CrossRef]
20. Wang, X.; Lim, L.T. A Kinetics and Modeling Study of Coffee Roasting Under Isothermal Conditions. *Food Bioprocess Technol.* **2014**, *7*, 621–632. [CrossRef]
21. Schenker, S. Investigations on the Hot Air Roasting of Coffee Beans. Ph.D. Thesis, ETH Zurich, Zurich, Switzerland, 2000. [CrossRef]
22. Alessandrini, L.; Romani, S.; Pinnavaia, G.; Rosa, M.D. Near infrared spectroscopy: An analytical tool to predict coffee roasting degree. *Anal. Chim. Acta* **2008**, *625*, 95–102. [CrossRef]
23. Vargas-Elias, G.; Correa, P.; de Souza, N.; Melo, E. Kinetics of Mass Loss of Arabica Coffee During Roasting Process. *Eng. Agríc.* **2016**, *36*, 300–308. [CrossRef]
24. Pramudita, D.; Araki, T.; Sagara, Y.; Tambunan, A.H. Roasting and Colouring Curves for Coffee Beans with Broad Time-Temperature Variations. *Food Bioprocess Technol.* **2017**, *10*, 1509–1520. [CrossRef]
25. Baggenstoss, J.; Poisson, L.; Kaegi, R.; Perren, R.; Escher, F. Roasting and aroma formation: Effect of initial moisture content and steam treatment. *J. Agric. Food Chem.* **2008**, *56*, 5847–5851. [CrossRef]
26. de Oliveira, G.H.H.; Corrêa, P.C.; Oliveira, A.P.L.R.d.; Baptestini, F.M.; Vargas-Elías, G.A. Roasting, Grinding, and Storage Impact on Thermodynamic Properties and Adsorption Isotherms of Arabica Coffee. *J. Food Process. Preserv.* **2017**, *41*, e12779. [CrossRef]

27. Rodrigues, C.; Correia, F.; Mendes, T.; Medina, J.; Figueira, C. CHAPTER 9 Post-roasting Processing: Grinding, Packaging and Storage. In *Coffee: Production, Quality and Chemistry*; The Royal Society of Chemistry: London, UK, 2019; pp. 258–271. [CrossRef]
28. Chu, B.; Yu, K.; Zhao, Y.; He, Y. Development of Noninvasive Classification Methods for Different Roasting Degrees of Coffee Beans Using Hyperspectral Imaging. *Sensors* **2018**, *18*, 1259. [CrossRef] [PubMed]
29. Chindapan, N.; Soydok, S.; Devahastin, S. Roasting Kinetics and Chemical Composition Changes of Robusta Coffee Beans During Hot Air and Superheated Steam Roasting. *J. Food Sci.* **2019**, *84*, 292–302. [CrossRef] [PubMed]
30. Al-Shemmeri, M.; Fryer, P.; Farr, R.; Lopez-Quiroga, E. Development of Coffee Bean Porosity and Thermophysical Properties During Roasting. *J. Food Eng.* **2024**, *378*, 112096. [CrossRef]
31. Fabbri, A.; Cevoli, C.; Alessandrini, L.; Romani, S. Numerical modeling of heat and mass transfer during coffee roasting process. *J. Food Eng.* **2011**, *105*, 264–269. [CrossRef]
32. Fadai, N.T.; Melrose, J.; Please, C.P.; Schulman, A.; Van Gorder, R.A. A heat and mass transfer study of coffee bean roasting. *Int. J. Heat Mass Transf.* **2017**, *104*, 787–799. [CrossRef]
33. Corradini, M.G.; Peleg, M. Prediction of vitamins loss during non-isothermal heat processes and storage with non-linear kinetic models. *Trends Food Sci. Technol.* **2006**, *17*, 24–34. [CrossRef]
34. Corradini, M.G.; Peleg, M. Linear and non-linear kinetics in the synthesis and degradation of acrylamide in foods and model systems. *Crit. Rev. Food Sci. Nutr.* **2006**, *46*, 489–517. [CrossRef]
35. Oliveira, L.; Hudebine, D.; Guillaume, D.; Verstraete, J. A Review of Kinetic Modeling Methodologies for Complex Processes. *Oil Gas Sci. Technol.* **2016**, *71*, 45. [CrossRef]
36. Schwartzberg, H. Modeling Bean Heating during Batch Roasting of Coffee Beans. In *Engineering and Food for the 21st Century*; CRC Press: Boca Raton, FL, USA, 2002. [CrossRef]
37. Zhu, M.; Long, Y.; Ma, Y.; Huang, Y.; Wan, Y.; Yu, Q.; Xie, J.; Chen, Y. Investigation of thermal contaminants in coffee beans induced by roasting: A kinetic modeling approach. *Food Chem.* **2022**, *378*, 132063. [CrossRef]
38. Schwartzberg, H. Modeling Exothermic Heat Generation during the Roasting of Coffee. In Proceedings of the 21st International Conference on Coffee Science, Montpellier, France, 11–15 September 2006.
39. Schwartzberg, H. Batch Coffee Roasting; Roasting Energy Use; Reducing That Use. In *Advances in Food Process Engineering Research and Applications*; Springer US: Boston, MA, USA, 2013; pp. 173–195.
40. Bottazzi, D.; Farina, S.; Milani, M.; Montorsi, L. A numerical approach for the analysis of the coffee roasting process. *J. Food Eng.* **2012**, *112*, 243–252. [CrossRef]
41. Schwartzberg, H. Improving Industrial Measurement of the Temperature of Roasting Coffee Beans. In Proceedings of the 21st International Conference on Coffee Science, Montpellier, France, 11–15 September 2006.
42. Bopape, N.; van der Merwe, A.; Vosloo, J.; Ross, R.G. Validation and Improvement of Heat and Mass Transfer Model in Prediciting the Coffee Roasting Profile. In Proceedings of the International Conference on Advances in Science, Engineering, Technology and Natural Resources, Parys, South Africa, 24–25 November 2016; pp. 225–232. [CrossRef]
43. Hernández Pérez, J.A. Modelling and Determining Coffee Roasting Quality on Line. Ph.D. Thesis, ENSIA (AgroParisTech), Paris, France, 2002. Available online: https://pastel.hal.science/pastel-00003699 (accessed on 15 October 2025).
44. Palma, F.D.; Iacono, F.; Toffanin, C.; Ziccardi, A.; Magni, L. Scalable model for industrial coffee roasting chamber. *Procedia Comput. Sci.* **2021**, *180*, 122–131. [CrossRef]
45. Vosloo, J. Heat and Mass Transfer Model for a Coffee Roasting Process. Master's Thesis, North-West University, Potchefstroom, South Africa, 2017.
46. Uren, K.R.; Vosloo, J.; van der Merwe, A.F.; van Schoor, G. Heat and mass transfer modeling of an artisan coffee roasting process: A comparative study. *Dry. Technol.* **2023**, *41*, 1697–1713. [CrossRef]
47. Alonso-Torres, B.; Hernández-Pérez, J.A.; Sierra-Espinoza, F.; Schenker, S.; Yeretzian, C. Modeling and Validation of Heat and Mass Transfer in Individual Coffee Beans during the Coffee Roasting Process Using Computational Fluid Dynamics (CFD). *Chimia* **2013**, *67*, 291–294. [CrossRef] [PubMed]
48. Oliveros, N.O.; Hernández, J.A.; Sierra-Espinosa, F.Z.; Guardián-Tapia, R.; Pliego-Solórzano, R. Experimental study of dynamic porosity and its effects on simulation of the coffee beans roasting. *J. Food Eng.* **2017**, *199*, 100–112. [CrossRef]
49. Al-Shemmeri, M.; Windows-Yule, K.; Lopez-Quiroga, E.; Fryer, P.J. Coffee bean particle motion in a spouted bed measured using Positron Emission Particle Tracking (PEPT). *J. Food Eng.* **2021**, *311*, 110709. [CrossRef]
50. Al-Shemmeri, M.; Windows-Yule, K.; Lopez-Quiroga, E.; Fryer, P.J. Coffee bean particle motion in a rotating drum measured using Positron Emission Particle Tracking (PEPT). *Food Res. Int.* **2023**, *163*, 112253. [CrossRef]
51. Che, H.; Al-Shemmeri, M.; Fryer, P.J.; Lopez-Quiroga, E.; Kokalova Wheldon, T.; Windows-Yule, K. PEPT validated CFD-DEM model of aspherical particle motion in a spouted bed. *Chem. Eng. J.* **2023**, *453*, 139689. [CrossRef]

52. Bustos-Vanegas, J.D.; Collazos-Escobar, G.A.; Gutiérrez-Guzmán, N.; Campos, T. Mathematical Modeling in Coffee Roasting: The Science Behind the Art. In *Proceedings of the Selected Topics in Food Process Engineering*; Vega-Castro, O.A., Simpson, R., Pilar Buera, M.d., Granda-Restrepo, D.M., Villa Zabala, C.C., Pinzón-Fandiño, M.I., Gutiérrez-López, G.F., Barbosa-Cánovas, G.V., Eds.; Springer: Cham, Switzerland, 2025; pp. 361–383.
53. Intercontinental Exchange. *Coffee "C" Futures Contract Rules (NYBOT No. 8)*; Technical Report; U.S. Commodity Futures Trading Commission: Washington, DC, USA, 2024. Available online: https://www.cftc.gov/sites/default/files/files/submissions/dcodcm/dcmnybotvcoffeec.pdf (accessed on 15 October 2025).
54. Levenspiel, O. Chemical reaction engineering. *Ind. Eng. Chem. Res.* **1999**, *38*, 4140–4143. [CrossRef]
55. Peleg, M.; Normand, M.D.; Corradini, M.G. The Arrhenius equation revisited. *Crit. Rev. Food Sci. Nutr.* **2012**, *52*, 830–851. [CrossRef]
56. Froessling, N. *The Evaporation of Falling Drops;* Defense Technical Information Center: Fort Belvoir, VA, USA, 1968; Volume 52, p. 37.
57. Brown, S.; Lattimer, B. Transient gas-to-particle heat transfer measurements in a spouted bed. *Exp. Therm. Fluid Sci.* **2013**, *44*, 883–892. [CrossRef]
58. Hobbie, M.; Eggers, R. The Influence of Endothermic and Exothermic Energies on the Temperature Field of Coffee Beans during the Roasting process. In Proceedings of the 19th International Scientific Colloquium on Coffee, Trieste, Italy, 14–18 May 2001.
59. Singh, P.C.; Singh, R.K.; Bhamidipati, S.; Singh, S.N.; Barone, P. Thermophysical properties of fresh and roasted coffee powders. *J. Food Process Eng.* **1997**, *20*, 31–50. [CrossRef]
60. Burmester, K.; Eggers, R. Heat and mass transfer during the coffee drying process. *J. Food Eng.* **2010**, *99*, 430–436. [CrossRef]
61. Cardoso, D.B.; Andrade, E.T.d.; Calderón, R.A.A.; Rabelo, M.H.S.; Dias, C.d.A.; Lemos, I.A. Determination of thermal properties of coffee beans at different degrees of roasting. *Coffee Sci.* **2018**, *13*. Available online: https://coffeescience.ufla.br/index.php/Coffeescience/article/view/1491 (accessed on 15 October 2025). [CrossRef]
62. Redgwell, R.J.; Trovato, V.; Curti, D.; Fischer, M. Effect of roasting on degradation and structural features of polysaccharides in Arabica coffee beans. *Carbohydr. Res.* **2002**, *337*, 421–431. [CrossRef]
63. Bergman, T.L.; DeWitt, D.P.; Incropera, F.; Lavine, A.S. *Fundamentals of Heat and Mass Transfer*; John Wiley & Sons: Hoboken, NJ, USA, 2011; Volume 997.
64. Engineering-ToolBox. Resources, Tools and Basic Information for Engineering and Design of Technical Applications, 2020. Available online: https://www.engineeringtoolbox.com/air-properties-d_156.html (accessed on 15 October 2025).

Disclaimer/Publisher's Note: The statements, opinions and data contained in all publications are solely those of the individual author(s) and contributor(s) and not of MDPI and/or the editor(s). MDPI and/or the editor(s) disclaim responsibility for any injury to people or property resulting from any ideas, methods, instructions or products referred to in the content.